EES Catalysis

REVIEW ARTICLE

View Article Online
View Journal | View Issue

Open Access Article. Published on 01 2568. Downloaded on 4/1/2569 10:24:58.
This article is licensed under a Creative Commons Attribution-NonCommercial 3.0 Unported Licence.

Check for updates

Cite this: *EES Catal.*, 2025, 3, 943

Unlocking the potential: key roles of interfacial water in electrocatalysis

Zheng Tang, Zhongliang Dong, Lingjie Yuan, Bowen Li and Yinlong Zhu *

Received 3rd June 2025,
Accepted 1st July 2025

DOI: 10.1039/d5ey00161g

rsc.li/eescatalysis

Interfacial water, serving as a subtle yet powerful performance modulator, plays a pivotal role in various electrochemical technologies due to its unique configurations and dynamic properties. Especially in the past decade, advances in electrocatalyst research, experimental characterization and theoretical modeling have significantly deepened the understanding of interfacial water's role in electrocatalytic systems. These as-obtained insights not only elucidate the dynamic behavior and structural properties of interfacial water but also highlight its importance in optimizing reaction pathways and improving electrocatalytic performance. Therefore, the understanding and regulation of interfacial water is an important topic in electrocatalytic research, and motivated us to compile this review. This review starts with a thorough analysis of interfacial water's properties and behaviors relevant to the electrocatalysis including structural types, water networks, rigidity and molecular orientation. Then, the specific roles of interfacial water in electrocatalysis are subsequently analyzed and classified as a co-catalyst, a masking agent, a regulator of reaction intermediates, and an inducer of catalyst reconfiguration. Next, some advanced experimental characterization and computational methods are presented to collectively probe the interfacial water, which is critical to capture accurate structural information. Furthermore, we present a comprehensive overview of key strategies for modulating the properties and behaviors of interfacial water to enhance the electrocatalytic performance of representative reactions at the electrolyte and catalyst levels, with emphasis on the specific mechanisms behind these modulation approaches. Finally, we discuss current challenges and future opportunities in this field, aiming to inspire the design of more advanced electrocatalytic systems.

Broader context

Water-mediated electrocatalytic technologies driven by renewable electricity occupy a central place in the future of clean energy conversion. Beyond its role as a proton source, water's unique interfacial properties critically influence electrocatalytic processes. Its properties such as structural types, molecular orientation and dynamic characteristics can significantly affect the proton transfer, intermediate stabilization and reaction kinetics in the electrocatalysis. A comprehensive understanding of interfacial water helps to provide insights into the electrocatalytic reaction mechanisms and provide ideas for the design of efficient electrocatalytic systems. This review begins with the presentation of the properties and behaviors of interfacial water relevant to electrocatalysis, and analyzes its impact on the electrocatalytic performance as well as mechanisms. In addition, this review summarizes the main characterization and theoretical approaches applied to study interfacial water and concludes with effective strategies to modulate interfacial water at the electrolyte and catalyst levels to enhance the electrocatalytic performance. Finally, current challenges and future opportunities in this field are discussed. This review is devoted to a comprehensive overview of the rapid progress of interfacial water research in the field of electrocatalysis, with the aim of providing prospective ideas and methods for electrocatalytic research.

1. Introduction

Water, a fundamental element on Earth, is not only essential for sustaining human civilization but also pivotal in advancing critical sectors such as agriculture, industry and energy production.[1–4] In the era of the global clean energy transition, electrocatalysis utilizing water as a medium has attracted widespread attention.[5,6] Water is an ideal carrier of both hydrogen and oxygen, and electrocatalysis technology provides an effective way to facilitate water splitting under mild conditions. Therefore, electrochemical hydrogenation and oxidative conversion processes with water as a medium have become gentle yet efficient methods for synthesizing high-value products.[7,8] As the cost of renewable electricity (particularly for the solar and wind energy) continues to decline, such transformative

Institute for Frontier Science, Nanjing University of Aeronautics and Astronautics, Nanjing 210016, China. E-mail: zhuyl1989@nuaa.edu.cn

© 2025 The Author(s). Published by the Royal Society of Chemistry

Open Access Article. Published on 01 2568. Downloaded on 4/1/2569 10:24:58.
This article is licensed under a Creative Commons Attribution-NonCommercial 3.0 Unported Licence.

technology is rapidly accelerating the shift towards a low-carbon economy, presenting a promising solution to the pressing global energy and climate challenges.[9–11]

Similar to the pivotal role of hydroelectric power and steam engines in past industrial revolutions, water is now integral to the 21st century's energy transition.[12,13] Since Mrs Fulhame's discovery in 1794 that water plays a non-consumptive role in metal reduction by hydrogen, our understanding of water in chemical reactions has advanced dramatically.[14] It was discovered that water can act as a "catalyst" or "mediator", not just a solvent or reactant. In addition to its widely recognized role as a proton source, emerging electrochemical technologies such as water electrolysis,[15–23] CO_2 conversion,[24–27] and nitrogen cycling,[28] extensively depend on the mysterious and unique properties of water. For instance, its distinct structure,[29,30] dynamic evolution,[31,32] unpredictable hydrogen bonding network reorganization,[33,34] rigid dimensions,[35] and profound orientation all play key roles in facilitating proton transfer,[33,36,37] modulating reaction intermediates,[16] and influencing the dynamics of solvation shells.[38] These interfacial phenomena have profound implications for electrocatalytic activity and reaction kinetics, underscoring the necessity of understanding water's behavior at the molecular level to improve the electrocatalytic performance and address the energy challenges.

Electrocatalysis occurs at the nanoscale interface between the electrocatalyst and electrolyte, known as the electrical double layer.[39,40] Interfacial water in this region forms a distinct layer with unique structural and dynamic properties, as shaped by the electric field and electrode surface.[41] Beyond acting as a solvent, interfacial water plays a critical role in proton transport, reactant adsorption and surface charge modulation, directly participating in reactions through electric field interactions.[42] Understanding its structure and dynamics is essential for optimizing the electrocatalytic systems. However, the study of interfacial water has been limited by experimental and theoretical challenges, as well as its inherent complexity and variability during reactions. Fortunately, recent advancements in catalyst research, experimental characterization techniques and theoretical models have led to a surge of interest in interfacial water. For example, Wang *et al.* obtained the first sub-molecularly resolved images of water molecules in real space.[43] Moreover, *in situ* shell-isolated nanoparticle-enhanced Raman spectroscopy, combined with *ab initio* molecular dynamics simulations, has for the first time provided insights into interfacial water's structures, including hydrogen-bonded water and Na^+-ion hydrated water.[41] Additionally, the combination of second harmonic (SH) and hyper-Raman scattering (HRaS) with nonlinear light scattering has enabled precise resolution of hydrogen bonds in water, allowing for the quantification of charge transfer and nuclear quantum effects (NQEs) in water molecules.[44] Interfacial water is now recognized as more than just a passive component of the reaction environment. Its unique structural orientation, hydrogen bonding network and dynamic reorganization considerably influence catalytic performance, reaction selectivity and the stability of intermediates. In recent decades, interfacial water research has achieved numerous breakthroughs as an important direction for developing novel regulatory strategies and revealing the potential mechanisms of electrocatalysis.[41,45–47] Therefore, a thorough review of the progress in interfacial water research is essential, systematically addressing its structural characteristics, dynamic behavior and specific roles in typical electrocatalytic reactions.

In this review, we present a comprehensive overview of interfacial water's key role in electrocatalysis, as schematically illustrated in Fig. 1. This review is structured in the following parts. We first present a detailed analysis of interfacial water's properties and behaviors relevant to electrocatalysis, encompassing its structural types, water networks, rigidity and molecular orientation. Next, the roles interfacial water play in the

Yinlong Zhu

Prof. Yinlong Zhu joined the Institute for Frontier Science at Nanjing University of Aeronautics and Astronautics (2022.1–present). He received his PhD degree from the College of Chemical Engineering at Nanjing Tech University in 2017, and then worked as a Discovery Early Career Researcher Award (DECRA) Fellow at Monash University, Australia (2017.12-2021/12). His current research focuses on the development of functional materials as high-performance electrocatalysts for the application of electrochemical energy conversion and storage technologies, such as fuel cells, metal–air batteries, water splitting and electrolyzers.

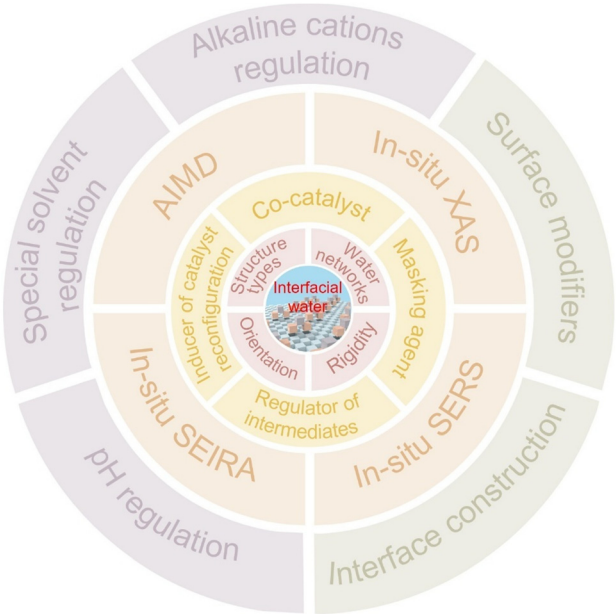

Fig. 1 Schematic illustration of interfacial water in electrocatalysis as summarized in this review, including basic properties, mechanistic insights of interfacial water, experimental characterization and computational methods and modulation strategies for enhanced electrocatalytic performance.

 © 2025 The Author(s). Published by the Royal Society of Chemistry

Open Access Article. Published on 01 2568. Downloaded on 4/1/2569 10:24:58.
This article is licensed under a Creative Commons Attribution-NonCommercial 3.0 Unported Licence.

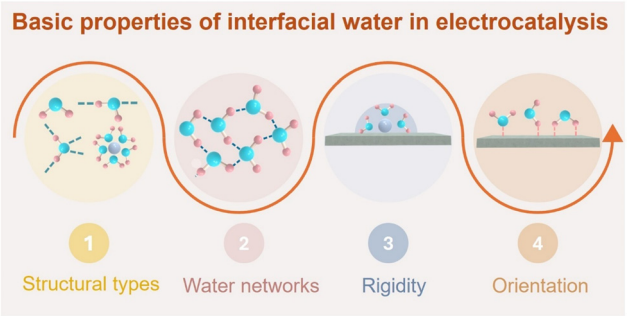

Fig. 2 Schematic illustration of basic properties of interfacial water in electrocatalysis.

electrocatalytic process are proposed including as a co-catalyst, a masking agent, a regulator of reaction intermediates and an inducer of catalyst reconfiguration. Subsequently, the development and application of some key experimental characterization techniques and theoretical simulations employed to study interfacial water are outlined, emphasizing their critical role in revealing the properties of interfacial water. Then, we explore several strategies for modulating the interfacial water properties and behaviors at the electrolyte and catalyst levels to improve the electrocatalytic activity, focusing on analyzing the specific mechanisms behind these modulation approaches. Lastly, some existing challenges in this emerging field and an outlook on future opportunities were provided. We believe that this comprehensive review will not only deepen our understanding of the critical role interfacial water in electrocatalysis but also provide valuable insights for the design of advanced electrocatalytic systems.

2. Basic properties of interfacial water in electrocatalysis

In electrocatalysis, interfacial water molecules play a key role in surface chemical reactions and mass transfer processes.[36,48] Influenced by the applied potential, nature of electrode surface, dissolved ions and other factors, the properties of water can be quite different from those in the bulk phase. The properties and behaviors of interfacial water including its structural types, hydrogen bonding network, rigidity and molecular orientation, exert a profound impact on the reactivity, stability and efficiency of electrochemical processes. In the following sections, we will explore each of these properties (Fig. 2) and examine the relationship with the electrocatalytic activity.

2.1. Structural types

The influence of interfacial water's structure on the electrocatalytic process remains an area of active research.[49,50] Water molecules are polar and have dipole moments, therefore they tend to be arranged in a complex network of hydrogen bonds.[51] These interactions create a dynamic and cooperative network of water molecules.[52] However, interfacial water molecules can be oriented to form localized structures in response to external stimuli under electrocatalytic conditions. These stimuli include

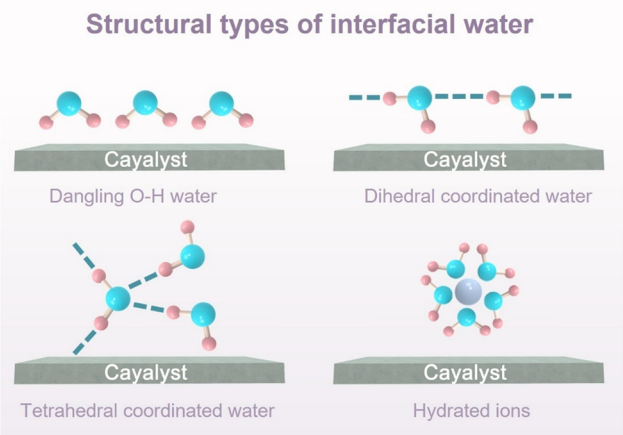

Fig. 3 Schematic illustration of structural types of interfacial water.

applied potentials, local pH, and surface charge, among others.[53] With advancements in coordination chemistry, catalytic studies and molecular dynamics simulations, specific coordination structures of water have been proposed to emphasize the interactions between water molecules and catalyst surfaces or other molecules at the molecular level.[54–57] The interfacial water's structure at the electrode–solution interface is categorized into four common types: dangling O–H water, dihedral coordinated water, tetrahedral coordinated water and hydrated ions (Fig. 3).

2.1.1. Dangling O–H water. In electrocatalysis, dangling O–H water molecules are characterized by weak interactions between their O–H bonds and atoms on the electrode or catalyst surface, with the other end suspended in the liquid phase. These dangling O–H groups facilitate proton transfer through the breaking and reformation of O–H bonds, promoting the activation and conversion of reactants.[58,59] In the case of dangling O–H water molecules, their interaction with the catalyst surface plays a crucial role in water dissociation into H^+ and OH^-. Impressively, Sun and colleagues thought that dangling O–H water molecules exhibit superior dissociation activity compared to other water configurations, which promotes superior HER performance.[29] Similarly, another study further confirmed the role of the excellent hydrolytic dissociation ability of dangling OH water on HER performance.[60] The increased content of dangling O–H water can reduce the energy potential for water dissociation and enhance the binding affinity of Pt atoms for active hydrogen intermediates, thereby leading to superior HER performance (Fig. 4a). Moreover, the excellent hydrolytic dissociation ability of dangling OH water facilitates a few hydrogenation reactions.[61,62] As shown in Fig. 4b, the dissociation of dangling O–H water accelerates the hydrogenation of *NO intermediates and efficiently converts NO_3^- to NH_3 through the Cl-coordination-induced center shift of the d-band of palladium atoms.[62]

2.1.2. Dihedral coordinated water. Dihedral coordinated water refers to water molecules that are linked to two other water molecules through hydrogen bonds, forming smaller aggregates. This type of coordination typically results in

Open Access Article. Published on 01 2568. Downloaded on 4/1/2569 10:24:58.
This article is licensed under a Creative Commons Attribution-NonCommercial 3.0 Unported Licence.

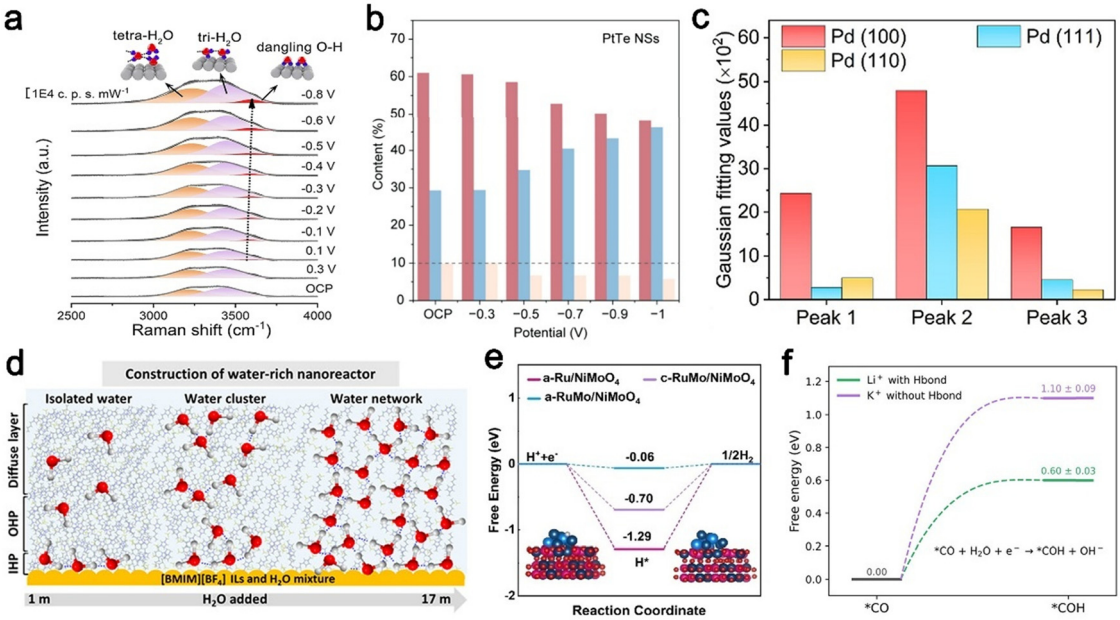

Fig. 4 (a) Raman shifts of various interfacial H_2O structures.[60] Copyright 2024, Nature Publishing Group. (b) Peak area content of three interfacial water structures on s-PtTe NSs catalysts.[62] Copyright 2024, American Chemical Society. (c) The peak area of 4-HB·H_2O, 2-HB·H_2O, and K·H_2O on Pd(100), Pd(111), and Pd(110).[63] Copyright 2023, American Chemical Society. (d) Schematic diagram of the aggregation state of water molecules with varying concentrations dispersed in the nonaqueous [BMIM][BF_4] ILs.[32] Copyright 2023, American Chemical Society. (e) Gibbs free energy diagram for a-Ru/$NiMoO_4$, a-RuMo/$NiMoO_4$ and c-RuMo/$NiMoO_4$ in the HER process.[67] Copyright 2025, Wiley-VCH. (f) Typical configurations representing the free energy diagram of *CO protonation.[73] Copyright 2024, American Chemical Society.

stronger adsorption of water on the catalyst surface, as each water molecule occupies two coordination sites with the metal surface. Despite its relatively low stability, dihedral coordinated water functions as a reaction intermediate or a structural transformer in certain electrocatalytic processes, influencing both the reaction rate and selectivity. For example, Ye *et al.* demonstrated the dihedral coordinated water on the Pd(100) surface effectively accelerates the semi-hydrogenation rate and improves olefin selectivity (Fig. 4c).[63] Analogously, tensile strain induced by PdCu icosahedral twins has been certified to facilitate the transformation of interfacial water structures.[64] The K–H_2O species promoted by tensile strain accelerates water splitting, thereby enhancing the efficiency of electrocatalytic semi-hydrogenation (ECSH), while dihedral-coordinated water contributes to improve olefin selectivity. Dihedral coordinated water molecules are thought to adopt a linear arrangement on the catalyst surface, maximizing electron cloud overlap. In the conversion of alkynes to olefins, the planar nature of olefins causes them to lie flat on the catalyst surface, leading to the significant repulsion with the surrounding water molecules. This spatial resistance promotes olefin desorption, thereby enhancing olefin selectivity in ECSH reactions.

2.1.3. Tetrahedral coordinated water. Tetrahedral coordinated water refers to water molecules connected to four other water molecules through hydrogen bonds, forming a highly ordered hydrogen bonding network. This configuration represents a common and robust hydrogen bonding water structure. Both dangling O–H water and tetrahedral coordinated water are crucial for electrocatalytic reactions, but their impacts differ. Dangling O–H water plays a pivotal role in proton transfer and hydrolysis processes, particularly for the HER wherein it enhances the electrocatalytic activity by increasing the proton transfer efficiency and lowering the reaction barrier.[29] In contrast, tetrahedral coordinated water promotes the reactant dissociation, electron transfer, and stabilization of reaction intermediates by providing a stable hydrogen-bonding network, thereby improving the electrocatalytic efficiency and selectivity.[65,66] For instance, Li *et al.* found that the hydrophobic tributyl ammonium bromide cation promotes the formation of an extended asymmetric tetrahedral coordinated network at the interface, facilitating OH^- transport through the Volmer step of the EDL and enhancing the HER performance (Fig. 4d).[32] Tetrahedral coordinated water could also accelerate the dynamic conversion of interfacial water and increase the electrocatalytic rate by leveraging its stable hydrogen bonding network. In a recent study, the amorphous and alloy structure of a-RuMo/$NiMoO_4$/NF modulates the interfacial water network.[67] As depicted in Fig. 4e, the modulated catalyst not only reduces the coordination number of surface atoms and improves interfacial charge distribution but also lowers the d-band center. Such transformation effectively induces the conversion of K^+–H_2O to tetrahedral coordinated water, thereby accelerating water dissociation and enhancing HER performance. These examples illustrate that tetrahedral coordinated water enhances the adsorption and dissociation of reactants through its stable hydrogen bonding network, thereby increasing the reaction rate.

2.1.4. Hydrated ions. Water, as a highly polar molecule, can interact with dissolved ions to form clusters through a

 © 2025 The Author(s). Published by the Royal Society of Chemistry

Open Access Article. Published on 01 2568. Downloaded on 4/1/2569 10:24:58.
This article is licensed under a Creative Commons Attribution-NonCommercial 3.0 Unported Licence.

process known as ionic hydration. These clusters, referred to as hydrated ions, arise from hydrogen bonding interactions between water molecules and ions, creating a "hydration shell" of water molecules around the ions.[68–70] Hydrated ions exhibit critical chemical and physical properties that influence the reaction rate, equilibria, and electrical conductivity. The earliest experimental work in this aspect can be traced back to Walther Nernst's transference experiments.[71] Hydrated ions have garnered widespread attention in electrocatalysis due to their ability to accelerate the reorganization of water networks under applied voltages, which leads to the enhanced charge transfer and improved electrocatalytic efficiency.[72] For example, Li *et al.*'s study reveals that water molecules bonded to cations at the interface are reorganized into a more ordered structure under the synergistic effect of cations and electrode potentials. This reorganization facilitates charge transfer between the electrode and water molecules, considerably enhancing the HER rate.[41] Hydrated ions can also modulate the dynamic behavior of water at the electrode/electrolyte interface.[73,74] For instance, larger cations can approach the interface through desolvation and partially coordinate with CO* and COH* species.[73] This environment prevents H atoms in surrounding interfacial water from interacting with oxygen atoms of interfacial water, effectively hindering further hydrogenation along the C_1 pathway (Fig. 4f).

2.2. Water networks

Due to its polar nature and curved molecular geometry, water molecules tend to form unique hydrogen bonds with each other, creating a three-dimensional water network. The water network is macroscopically disordered as a whole due to its dynamic qualities, but water molecules receive external influences that usually realize local structures.[75,76] Water networks play a key role in electrocatalysis, directly affecting reaction kinetics, stability of intermediates and overall electrochemical efficiency. For instance, Luo *et al.* proved that the structurally ordered interfacial water molecules promote efficient proton-coupled electron transfer across the interface, lowering the energy barrier for subsequent dissociation processes.[31] The water networks will also interact with ions in solution to achieve microenvironmental regulation.[77] For instance, Li *et al.* pointed out that when amphiphilic cationic surfactants are used to reorganize interfacial water, an ordered assembly is formed at the charged electrode–electrolyte interface. This kind of interfacial microenvironment realizes the enrichment of CO_2 and increases the selective electroreduction of CO_2 to CO (Fig. 5a). In addition, the dynamic nature of the water network allows for rapid reconfiguration in response to changing electrochemical conditions. Changes in localized hydrogen bonding can alter the electrostatic interactions between the electrocatalyst and the adsorbed substances, thereby affecting their adsorption energies and reaction kinetics. For example, at high negative polarization potentials, the water networks are induced by hydrophobic cations to form a relatively disordered asymmetric tetrahedral coordinated water network. Compared with the strongly hydrogen-bonded tetrahedral coordinated water network, the tetrahedral coordinated water network has a shorter distance to the catalyst, which facilitates the OH^- migration on the EDL in the Volmer step.[32] Additionally, disrupting the high connectivity of the water network can effectively modify the water structure to regulate proton dynamics.[78] Impressively, Peng *et al.* disrupted the stringent hydrogen bonding network by introducing harder Lewis acids (*e.g.*, ZrO_2, TiO_2, and HfO_2), thereby promoting efficient proton transport and improving the OER activity (Fig. 5b).[33]

2.3. Rigidity

The rigidity of the interfacial water layer is a structural characteristic that reflects the behavior of hydrogen bonds at the interface. Due to the structural constraints imposed by the surface, the rigidity is closely associated with the density and reorientation of these hydrogen bonds. Specifically, as the system approaches the zero free-charge potential, the hydrogen bonds tend to be more capable of reorienting, which can facilitate the recombination. Conversely, the farther the system moves from this potential, the more rigid the water becomes, thereby hindering its reorganization.[35] Under acidic and alkaline conditions, the ordination and rigidity of the interfacial water are significantly reduced due to the influence of H^+ and OH^-, which leads to localized hydrogen bond breaking and dynamic reorganization. In contrast, interfacial water in neutral media forms a highly ordered tetrahedral network structure through dense hydrogen bonding and tends to be stiffer than interfacial water layers in acidic and alkaline media.[79] Rigid interfacial water forms a dense network of hydrogen bonds that may prevent reactants from approaching the catalyst surface and reduce mass transfer efficiency. However, its qualities may optimize intermediate adsorption and stabilize certain intermediates in a directed arrangement, making it suitable for reactions that require stabilization of intermediates.[25] For example in the CO_2RR, strong intermolecular hydrogen bonds make it difficult to reorient the water, resulting in longer metal–H distances, which inhibits hydrolysis and reduces H* coverage. A moderate H* coverage not only inhibits the HER, but also ensures the hydrogenation of intermediates, thus facilitating C–C dimerization with a schematic of the hydrogen bonding structure of interfacial water shown in Fig. 5c.

2.4. Orientation

Interfacial water orientation plays a critical role in electrocatalysis, which refers to the alignment of water molecules at the catalyst–electrolyte interface.[80] Since water molecules reorient themselves rapidly in response to hydrogen bond donor–acceptor interactions, the orientation of interfacial water is far more intricate than previously anticipated.[81–83] The orientation can significantly influence the reactivity, proton conduction, and overall reaction mechanism. It is found that when the interfacial water molecule adopts the "H-down" orientation, it forms a configuration with O–H bonds pointing to the active site. The "H-down" orientation allows H^+ to jump directly to the surface of the catalyst through the hydrogen-bonding network, and drastically reduces the proton transfer energy barrier.[45,84] Remarkably,

Open Access Article. Published on 01 2568. Downloaded on 4/1/2569 10:24:58.
This article is licensed under a Creative Commons Attribution-NonCommercial 3.0 Unported Licence.

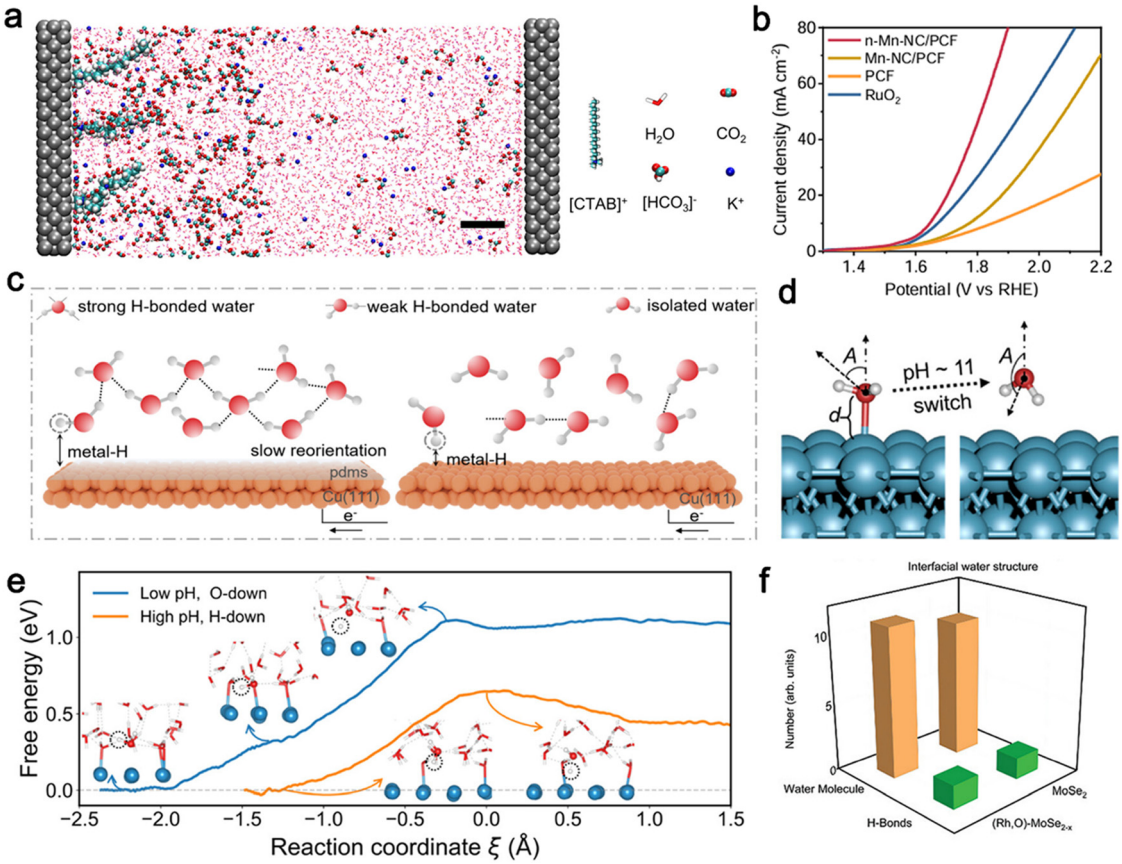

Fig. 5 (a) Snapshot of aqueous solution with salt added between two planar Ag electrodes in the CTAB-containing system from MD simulation.[77] Copyright 2022, American Chemical Society. (b) OER LSV polarization curves measured in 0.1 M PBS solution.[33] Copyright 2025, Wiley-VCH. (c) Schematics of the hydrogen bonding structure of interfacial water in Cu(111)@PDMS and Cu(111) under bias potential.[25] Copyright 2024, American Chemical Society. (d) Structural models of low-pH and high-pH water configurations on Pt(111). (e) The free energy profile of water dissociation for H-down water at high pH and "O-down" water at low pH.[85] Copyright 2024, American Chemical Society. (f) The average number of hydrogen bonds per interfacial water molecule for $MoSe_2$ and (Rh, O)−$MoSe_{2-x}$ models.[37] Copyright 2024, Wiley-VCH.

Tian *et al.* obtained the Raman signals of interfacial water for the first time on the surfaces of Au(111) and (100) single-crystal electrodes. *In situ* two configurational transitions of interfacial water during the HER were observed: the interfacial water changes from a "parallel" structure to a single "H-down" and then to a double "H-down" structure as the potential shifts negatively, significantly enhancing the HER rate.[36] Besides, a similar phenomenon is also observed by Chen *et al.* in characterizing the surface-limited interfacial water molecule structure of graphene.[84]

Interfacial water is very sensitive and its orientation is influenced by a number of factors. For example, a kinetic investigation of the HER on Pt surfaces at different pH values reveals that the orientation of interfacial water shifts from an "O-down" configuration below pH 10 to an "H-down" configuration above pH 10 (Fig. 5d and e).[85] Furthermore, Ren *et al.* found the electron-rich environment on the O atoms induces a conformational change of interfacial water molecules from "O-down" to "H-down," resulting in a disordered interfacial water network (Fig. 5f).[37] It is also worth noting that the orientation kinetics in finite space and *in vivo* are quite different, since the dipole-related relaxation time of H_2O molecules in narrow CNTs has been reported to be much slower than that of native water, and these orientation kinetics will significantly affect the chemical activity and proton transfer of water.[86]

3. Mechanistic insights of interfacial water in electrocatalytic reactions

Interfacial water exhibits remarkable advantages in electrochemical research due to its unique physicochemical properties, including its diverse molecular forms, exceptional solvent capacity, efficient mass transport and moderate reactivity. In the last few decades, a great deal of work has prioritized customizing catalyst structures while overlooking the influence of water molecular structure on catalytic mechanisms and performance. Over recent years, with the advancement of high temporal and spatial resolution spectroscopy, the effect of water structure on electrocatalytic mechanism and performance has attracted widespread attention. Therefore, we will next explore the function of interfacial water in several types of

 © 2025 The Author(s). Published by the Royal Society of Chemistry

Open Access Article. Published on 01 2568. Downloaded on 4/1/2569 10:24:58.
This article is licensed under a Creative Commons Attribution-NonCommercial 3.0 Unported Licence.

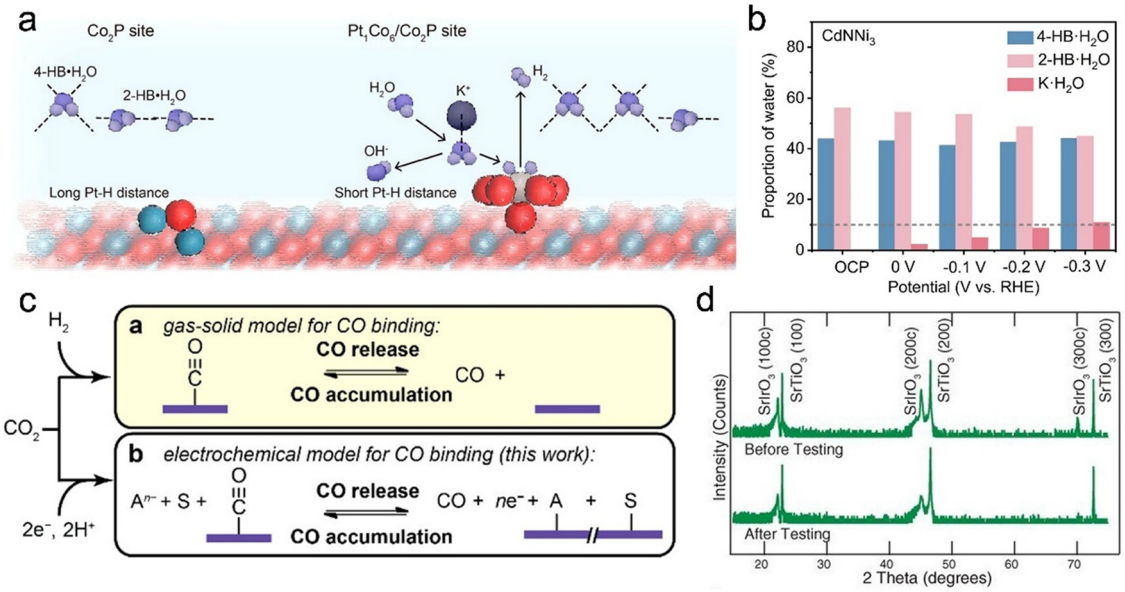

Fig. 6 (a) Illustration of HER mechanisms.[87] Copyright 2025, Wiley-VCH. (b) Peak area proportion of three interfacial water structures (4-HB·H_2O, 2-HB_2O and K·H_2O) on $CdNNi_3$.[94] Copyright 2025, Wiley-VCH. (c) Gas–solid model and electrochemical model for CO binding.[97] Copyright 2021, American Chemical Society. (d) XRD of a 100-nm $SrIrO_3$ film before and after 30 hours of OER testing.[102] Copyright 2016, American Association for the Advancement of Science.

conventional electrocatalytic reactions (*e.g.*, HER, OER, CO_2RR, and NO_3^-RR).

3.1. As a co-catalyst

Due to its unique structural and dynamic properties, interfacial water acts as a co-catalyst in electrocatalysis, significantly affecting the electrocatalytic activity. One of the features is to act as a proton transfer medium by adjusting the structure, rigidity, and orientation of the interfacial water at the microscopic level and reorganizing the hydrogen bonding network at the macroscopic level. For example, Tan *et al.* found that the strongly-negative charged Pt_1Co_6 configuration optimizes the reorganization of the interfacial water structure. Elevated concentrations of hydrated K^+ accelerate proton transport by enhancing Pt–H binding interactions and facilitating H–OH bond polarization, which increase HER activity (Fig. 6a).[87] Besides, Zhai *et al.* reconstructed the connected hydrogen bonding network between the Mn–Co_3O_4@CN-electrolyte interface by coupling hydrophilic units. Hydrogen bonding interactions between CN units and H_2O molecules promote proton enrichment and thus the dehydrogenation process.[88] In addition, interfacial water can generate active sites through interaction with the electrocatalyst.[89] Impressively, when they interact with surface hydroxyl oxides in the OER, the hydrophilic nature of the surface has been shown to accelerate the rate of charge transfer between the electrolyte and the electrode, thereby enhancing OER activity.[90] Furthermore, interfacial water molecules also interact with solution ions. During electrocatalysis, the high mobility of water molecules promotes efficient transport of charged species across the electrode surface, thereby minimizing the kinetic barriers associated with mass transfer.[91]

3.2. As a masking agent

In electrocatalytic reactions, water plays a distinctly dual role, acting either as a promoter or as an inhibitor of the reaction. Water molecules exhibit a strong adsorption capacity on the electrode surface, potentially competing with reaction substrates (*e.g.*, CO_2, O_2) or intermediates for access to active sites. For instance, it has been observed that an excess of water can cover pt active sites, thereby hindering O_2 adsorption and electron transfer.[92] Additionally, it has been suggested that an overabundance of interfacial water may result in the unavailability of active sites on the electrocatalyst surface or impede gas diffusion. Such challenges often necessitate the modulation of the local density of interfacial water to maintain the hydrophobicity of the electrode surface, a topic that will be addressed in Section 5.2.1. In the OER, interfacial water may also induce the oxidation of certain metal catalysts during the catalytic process, consequently leading to a reduction in catalytic activity.[93] In neutral media, interfacial water forms a dense hydrogen bonding network, making it harder than in acidic or alkaline conditions, which can hinder reactants from reaching the catalyst surface and lower mass transfer efficiency.[79]

3.3. As a regulator of reaction intermediates

The interaction among interfacial water, intermediates, and electrocatalysts can modify the binding strength between intermediates and catalytic sites, thereby influencing the adsorption of reaction intermediates. This modulation attenuates the excessive adsorption of intermediates on the catalyst surface. In a recent study, we modulated the electronic structure of antiperovskites through an A-site tuning strategy to facilitate a shift in the conformation of interfacial water. The transition

Open Access Article. Published on 01 2568. Downloaded on 4/1/2569 10:24:58.
This article is licensed under a Creative Commons Attribution-NonCommercial 3.0 Unported Licence.

from 2-HB–H_2O to K–H_2O is more conducive to the dissociation of adsorbed water, thereby enhancing HER activity (Fig. 6b).[94] In addition, it can be useful to study interfacial water in a wider range of reaction systems, such as the CO_2RR, which are more complex and challenging than the HER.[95] The interaction of interfacial water with intermediates will directly affect the reaction pathway. For example, Zhang *et al.* disrupted the hydrogen bonding of interfacial water and reduced H_2O activity to affect *CO surface coverage, revealing the role of interfacial water in controlling the branching between the C_1 and C_2^+ pathways in the CO_2RR.[96] As another example, water adsorption contributes to the release of CO from the Au catalyst, hindering further reduction. In contrast, carbonate desorption helps CO to accumulate on Cu to permit further reduction to C_2 products (Fig. 6c).[97] Furthermore, for multi-step pathway reaction processes, interfacial water can modulate the H* adsorption capacity in addition to accelerating water dissociation to ensure sufficient H* on the catalyst surface.[28,98]

3.4. As an inducer of catalyst reconfiguration

Structural reconstruction due to dynamic interactions between water and electrocatalysts in an electrochemical environment is a core determinant of catalyst stability and activity. This process involves complex phenomena such as surface atomic rearrangements, phase transitions, and dissolution/redeposition.[99] This structural reconstruction can be driven by factors such as changes in potential, pH and reactant concentration.[100,101] In the OER, high oxidizing conditions induce surface oxidation or phase transition of metal oxides, which can enhance electrocatalytic activity and stability. One example is the $IrO_x/SrIrO_3$ catalyst which underwent leaching of Sr after the OER with the formation of IrO_3 or IrO_2 on the surface (Fig. 6d).[102] Water can also contribute to the stabilization of specific catalytically active substances, facilitating specific fundamental reaction steps that enhance performance. For example, the presence of water can lead to the formation of hydrated substances or hydroxylated surfaces, which typically creates more active sites for electrochemical reactions.[103] In reduction reactions, oxide catalysts may be reduced to the metallic state, accompanied by dramatic shifts in surface composition, electronic structure and morphological structure. For instance, Xiao *et al.* found that the kinetics and thermodynamics of CO_2 adsorption/activation and CO coupling are significantly improved when Cu^+ is partially reduced to Cu^0.[104] The remodeling phenomena have also been discovered for HER catalysts. For example, Gao *et al.* investigated the surface remodeling of Mo_2C–MoO_x: from Mo(VI) to Mo(IV) and achieved enhanced HER in 1 M $HClO_4$.[105]

4. Advanced experimental characterization and computational methods

There has been significant progress in methods for characterizing interfacial water with the continuous advancement of science and technology as well as the improvement of experimental equipment. In the last decade, modern techniques such as scanning tunneling microscopy (STM), *in situ* vibrational spectroscopy, and X-ray absorption spectroscopy (XAS) have greatly enhanced the accuracy, reliability, and resolution of experiments, offering higher dynamic, spatial, and temporal precision.[106–108] Compared to other methods, spectroscopy provides a more comprehensive and flexible understanding of water molecule behavior on catalyst surfaces, making it an indispensable tool in the research of interfacial water.[109,110] However, no single technique can fully capture the complex and dynamic behavior of interfacial water. The development of *ab initio* molecular dynamics (AIMD) has introduced a powerful theoretical tool for studying interfacial water, enabling detailed atomic-level insights into water molecules on the electrocatalyst surface.[111–113] By offering atomic-level details on the local structure of interfacial water, electron density distribution and electronic interactions with the catalyst surface, AIMD provides valuable insights into key phenomena such as adsorption, desorption, structural changes, solvent effects, and the interaction of water in the electrocatalytic processes. In this section, we will focus on the most widely used techniques for studying interfacial water: *in situ* XAS, *in situ* surface-enhanced Raman spectroscopy (SERS), *in situ* surface-enhanced infrared spectroscopy (SEIRAS), and AIMD. These methods provide critical insights into the structural and dynamic properties of interfacial water, advancing our understanding of its role in electrocatalytic systems.

4.1. *In situ* XAS

As displayed in Fig. 7a, XAS including X-ray absorption near-edge structure (XANES) and extended X-ray absorption fine structure (EXAFS), provides critical insights into interfacial water in the electrocatalysis.[47] For example, XANES reveals how interfacial water influences the electronic states of electrocatalyst surface, enhancing our understanding of water's electronic effects on electrocatalytic reactions.[114,115] By combining XANES with EXAFS, it is possible to gain a deeper insight into the effect of interfacial water on the electrocatalytic activity and reaction mechanism. A previous XAS-based study has shown that the concentration of hydrogen bonds, in the first few aqueous layers near the electrode surface, is significantly lower than in bulk water. Specifically, half of the interfacial water molecules exhibit fully saturated hydrogen bonds within about 1 nm from the electrode. In contrast, the other half are hydrogen-bonded and broken, which provide early evidence of the dynamic structural evolution of interfacial water.[114] Subsequent studies further elucidated the structural changes of interfacial water during electrocatalysis, providing detailed mechanistic insights. For instance, Zhang *et al.* employed *in situ* XAS to demonstrate that the valence state of Cu_2Cl_2-$(BIANP)_2$ decreases with a new coordination mode appearing at 1.4 Å (Fig. 7b).[28] The presence of Cl significantly influences the concentration of K–H_2O on the electrocatalyst surface, which can enhance water dissociation and generate more reactive H*, thereby further facilitating the multi-step hydrogenation of NO_3^- to NH_3. Similarly, FT-EXAFS analysis reveals an increased radial distance in the Pt–O (L) configuration, suggesting that

 © 2025 The Author(s). Published by the Royal Society of Chemistry

Open Access Article. Published on 01 2568. Downloaded on 4/1/2569 10:24:58.
This article is licensed under a Creative Commons Attribution-NonCommercial 3.0 Unported Licence.

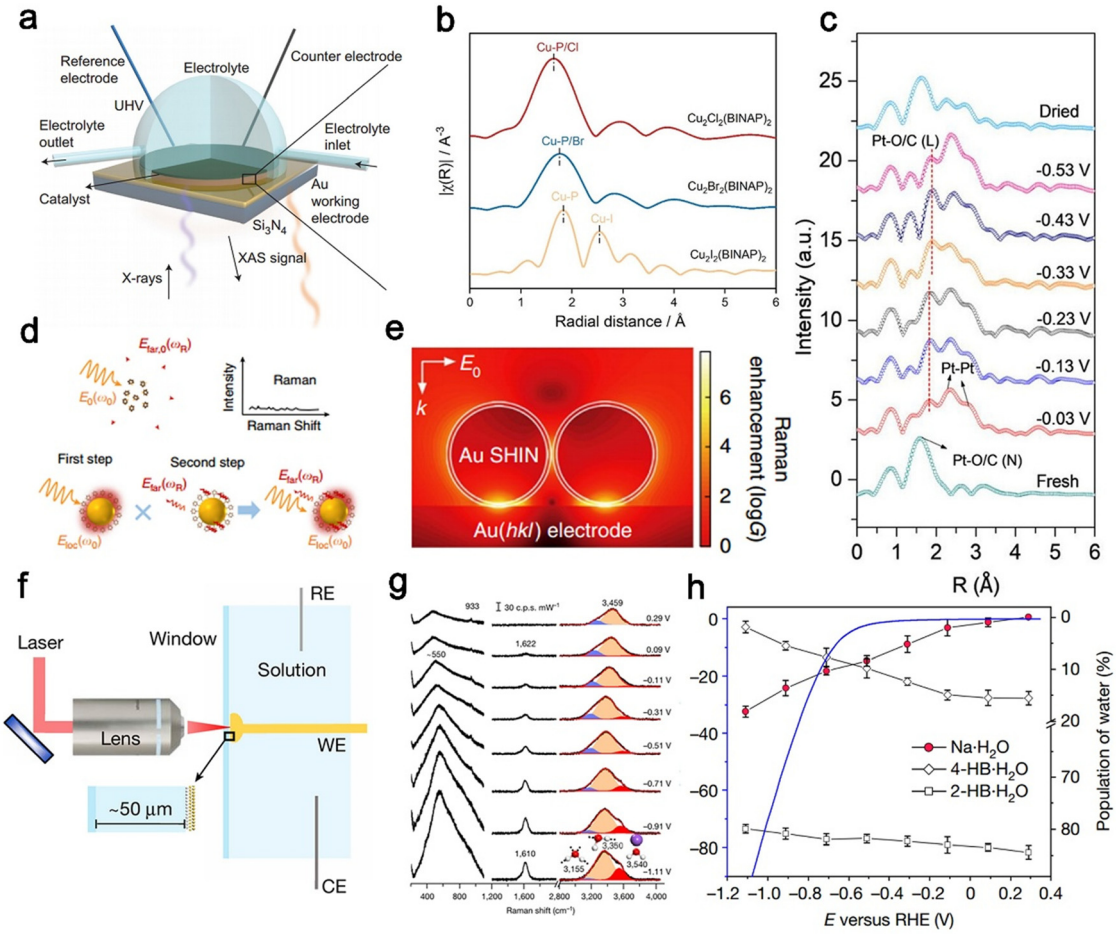

Fig. 7 (a) Schematic presentation of the *in situ* XAS.[47] Copyright 2017, Nature Publishing Group. (b) RSFs of the CHCs obtained from the EXAFS spectra.[28] Copyright 2025, Wiley-VCH. (c) *Operando* FT-EXAFS spectra of SNM-Pt at different potentials during the HER.[116] Copyright 2021, American Chemical Society. (d) Normal Raman scattering $E_{far,0}(\omega_R)$ and Raman spectrum of molecules illuminated by a narrow band laser.[102] Copyright 2021, Nature Publishing Group. (e) 3D-FDTD calculation of the Raman enhancement distribution of the coupling configuration between the Au surface and a 2 × 2 array of Au SHINs.[45] Copyright 2019, Nature Publishing Group. (f) Schematic of the Raman experimental setup. (g) *In situ* Raman spectra of interfacial water on a Pd(111) electrode in a 0.1 M $NaClO_4$ solution (pH 11). (h) Potential-dependent population of interfacial water from *in situ* Raman spectra and HER current density.[41] Copyright 2021, Nature Publishing Group.

the evolution of interfacial water from an "O-near" to an "O-far" configuration accelerates the proton transfer and reaction rate (Fig. 7c).[116] Additionally, XAS and ambient pressure X-ray photoelectron spectroscopy (AP-XPS) confirms that $Mo^{\delta+}$ sites enhance the adsorption and activation of interfacial water, thus contributing to the remarkable activity.[117,118]

4.2. *In situ* SERS

The observation of intense Raman signals from pyridine on roughened Ag electrodes marked the discovery of surface-enhanced Raman scattering (SERS).[119] In contrast to conventional Raman scattering, SERS leverages the optical properties of nanostructures with plasmonic characteristics, which leads to a substantial enhancement of the Raman signals from target molecules located in close proximity to the plasmonic metal nanostructures (Fig. 7d).[120] This enhancement is linked to surface plasmon resonance (SPR), where a rough electrode surface is required.[121,122] Noble metals like Ag, Au, and Cu, as well as non-metallic materials such as transition metals, semiconductors and graphene, are able to generate significant SERS effects.[123] The key advantage of SERS is its ability to amplify signals from species adsorbed on metal nanostructures while minimizing interference from bulk solution molecules, thereby making SERS a powerful tool for studying the dynamic evolution of interfacial water structures and catalyst surfaces.[124,125]

However, traditional SERS substrates confront the limitations in spatial resolution and interference between sample molecules and the substrate. To address this, plasma-enhanced Raman spectroscopy (PERS), including shell-isolated nanoparticle-enhanced Raman spectroscopy (SHINERS), has been developed.[126] Tian *et al.* pioneered ultra-thin, non-porous inert shell layers to encapsulate nanoparticles, overcoming substrate material limitations and enabling the first Raman detection of interfacial water on Au(111) single-crystal electrodes (Fig. 7e).[45] Based on this, Li *et al.* designed a vertical electrochemical Raman cell to reduce hydrogen bubble interference during *in situ* measurements (Fig. 7f).[41] They found that interfacial water consists of hydrogen bonding networks and hydrated

Open Access Article. Published on 01 2568. Downloaded on 4/1/2569 10:24:58.
This article is licensed under a Creative Commons Attribution-NonCommercial 3.0 Unported Licence.

Na^+, which dynamically translates from disordered to ordered configurations under HER conditions. The ordered structure can facilitate efficient electron transfer, consequently enhancing the HER activity (Fig. 7g and h). These studies significantly advance the use of SERS in characterizing interfacial water, providing key insights into its role in interfacial reactions and electrochemical kinetics.

Despite these advancements, the field of macro-optical design for SERS is still emerging. Future progress could depend on advanced strategies to fabricate nano/microstructures that optimize the SERS effect. For macroscopic optics, scanning microsphere microscopy, which has received much attention in recent years, converges excitation light into nano-jets through microscale dielectric spheres.[127,128] The combination of scanning microspheres and plasma-enhanced substrates is expected to broaden the application areas of SERS.[129]

4.3. *In situ* SEIRAS

The discovery of the surface-enhanced infrared absorption (SEIRA) effect dates back to the pioneering work of Hartstein *et al.*, who observed a significant amplification of the infrared absorption signal of nitrobenzoic acid films on silicon substrates in the presence of Ag or Au.[130] Initially identified on noble metal films like Au, Ag, and Cu, the SEIRA phenomenon is later extended to other metals such as Pt, Sn, Pd and In, which form nanostructured island layers on substrates. When samples are adsorbed onto these metal films and illuminated with photons at resonant frequencies, the localized light field's energy density increases, enhancing the absorption rate per unit volume. In recent years, SEIRAS has experienced rapid advancements driven by progressive research efforts.[131–134]

Similar to SERS, SEIRAS leverages plasmonic surface enhancement effects to significantly improve the surface selectivity. When irradiated with light near the plasmon resonance frequency, an intensified electromagnetic field is generated around metal nanoparticles supported by a solid substrate. This localized field confined to a few nanometers, dominates the overall signal to make SEIRA highly sensitive to surface phenomena (Fig. 8a).[134] By using this technique, localized hydrogen bonding states of water near metals and self-assembled membranes were found.[135–137] To better understand how interfacial water structures influence the electrocatalytic processes, *in situ* SEIRAS has become increasingly important.[138] *Via in situ* SEIRAS, it has been demonstrated that water molecules at the interface form an enhanced hydrogen bonding network in neutral media, hindering the transport of H_2O^*/OH^* species and enhancing HER activity (Fig. 8b and c).[16] Similarly, Zhou *et al.* confirmed that the rigid water networks around Li^+ restrict hydrogen atoms from approaching adsorbed CO_2, while the more flexible network around larger cations like Na^+ facilitates water reorientation and thereby enhances hydrogen proximity to CO_2 (Fig. 8d and e).[24]

Macro-optics design should not only be suitable for nano-/micro-optics design, but also for practical applications. Nano-infrared spectroscopy has improved spatial resolution to the nanometer scale, but it has difficultly working in aqueous environments. Recently, the ATR prism-coupled optics partially overcame the limitations of nano-IR spectroscopy and imaging in liquid environments.[139,140] These innovations enable more precise characterization of interfacial water's dynamics, paving the way for a deeper understanding of its role in electrocatalytic processes.

4.4. Other characterization techniques

In addition to the above main characterization techniques, other effective techniques such as the STM, atomic force microscope (AFM), solid-state nuclear magnetic resonance (SSNMR) and dynamic contact angle (DCA) also play an important role in the study of interfacial water's substructure, arrangement and orientation.[137,141–143] For example, STM can analyze the electronic properties of water molecules at interfaces and observe the dynamics of interfacial water under different environmental conditions. The high-resolution images of the surface topography help to observe the arrangement of interfacial water molecules and their interaction with the solid surface provided by AFM. However, all these experimental characterization techniques have their own limitations. For example, SSNMR is less sensitive compared to other techniques and may not accurately detect interfacial water at low concentrations. STM is limited in its application to electrocatalysts with high specific surface area or complex surface structures. Therefore, in order to more accurately explain the properties of interfacial water in electrocatalysis, multiple characterization techniques need to be employed simultaneously to comprehensively analyze the structure, orientation and dynamic evolution of interfacial water molecules.

4.5. AIMD

While traditional experimental techniques such as XAS, SERS and SEIRAS provide valuable insights into the structure of interfacial water, they are limited in capturing dynamic behavior and molecular-scale interactions. Classical molecular dynamics, widely used to characterize key properties of liquids at interfaces, relies on parameterized force fields and is not optimized for interfacial systems.[144,145] AIMD is not constrained by these limitations and provides an atomic-level description of interactions between water molecules and electrocatalyst surfaces, offering insights into adsorption modes, structural changes, and electronic states. By simulating the adsorption, desorption, and reaction processes of water on the catalyst surfaces, AIMD predicts water's behavior and structure under various reaction conditions, especially for some cases that are difficult to observe experimentally.

As a crucial complementary tool, AIMD has been applied to study the structure of water and electronic energy levels at electrochemical interfaces.[146] For example, Tuckman *et al.* used AIMD simulations to investigate the solvation state of protons in water, demonstrating the presence of intrinsic and Zundel cations and revealing the ordering of local water molecule structures.[147] Selloni *et al.* explored the dynamics of excess electrons at the TiO_2–water interface, showing the facet-dependent electrocatalytic behavior consistent with experimental observations.[148] Besides, AIMD has proven particularly valuable for studying the structural and dynamical characteristics of water molecules, which are often challenging to probe experimentally. For instance, Sautet *et al.*

 © 2025 The Author(s). Published by the Royal Society of Chemistry

Open Access Article. Published on 01 2568. Downloaded on 4/1/2569 10:24:58.
This article is licensed under a Creative Commons Attribution-NonCommercial 3.0 Unported Licence.

utilized AIMD to characterize the water and γ-Al_2O_3(110) interface at the atomic scale, revealing significant reorganization of proton distribution within the chemisorbed water layer and its great influence on electrocatalytic mechanisms.[149] Water molecules exhibit distinct angular orientations, with translational self-diffusivity reduced by up to two orders of magnitude and angular relaxation time increased by as much as sixfold. At the same time, AIMD calculations are increasingly being utilized to guide the design of catalysts.[46] The H_2O molecules at the customized Ru/Nb_2O_5 interface were reoriented due to the negatively charged regions, which increased the free water near Ru and improved the HER activity under neutral conditions (Fig. 8f).

AIMD provides a critical theoretical framework for studying the properties of interfacial water and reaction mechanisms, offering precise atomic-level insights into dynamic hydrogen bonding network evolution and conformational changes.[150] With continued advancements in computational power and algorithms, AIMD is expected to be able to significantly enhance our understanding of molecular interactions at interfaces, contributing to the design of new electrocatalysts and the optimization of electrocatalytic interfacial microenvironments.

5. Modulation strategies for enhanced electrocatalytic performance

As reported, significant progress in the last decade has been made in the design of high-performance electrocatalytic systems by modulating interfacial water's properties.[29,32,73,85] In this section, we will summarize some representative strategies for modulating interfacial water to improve the electrocatalytic performance (Fig. 9) and enhance the understanding of the key role of interfacial water in electrocatalysis from the perspectives of both the electrolyte (including alkali cation regulation, special solvent regulation, and pH regulation) and electrocatalyst (including surface modification and interface construction).

5.1. Electrolyte aspect

The electrolyte can modulate the properties of interfacial water, mainly because the solvent, solutes, and special additives in the electrolyte as well as their interactions can significantly affect the structure, kinetics, and chemistry of the interfacial water. For example, solvent molecules (*e.g.*, water and organic solvents) and solute ions (*e.g.*, Li^+, Na^+ and K^+) in the electrolyte form a stable shell layer through solvation, and this solvation can change the arrangement of interfacial water molecules and hydrogen bonding network.[151] Furthermore, the cations in the electrolyte can affect the structure and properties of the interfacial water through radius and size.[152] In this section, we summarize three main methods from the electrolyte aspect, which include alkaline cation regulation, special solvent regulation and pH regulation.

5.1.1. Alkaline cation regulation. Alkali cation regulation refers to the phenomenon wherein cations in alkaline environments influence the structural, chemical and dynamic properties of water molecules at solid surfaces or electrode interfaces.[153]

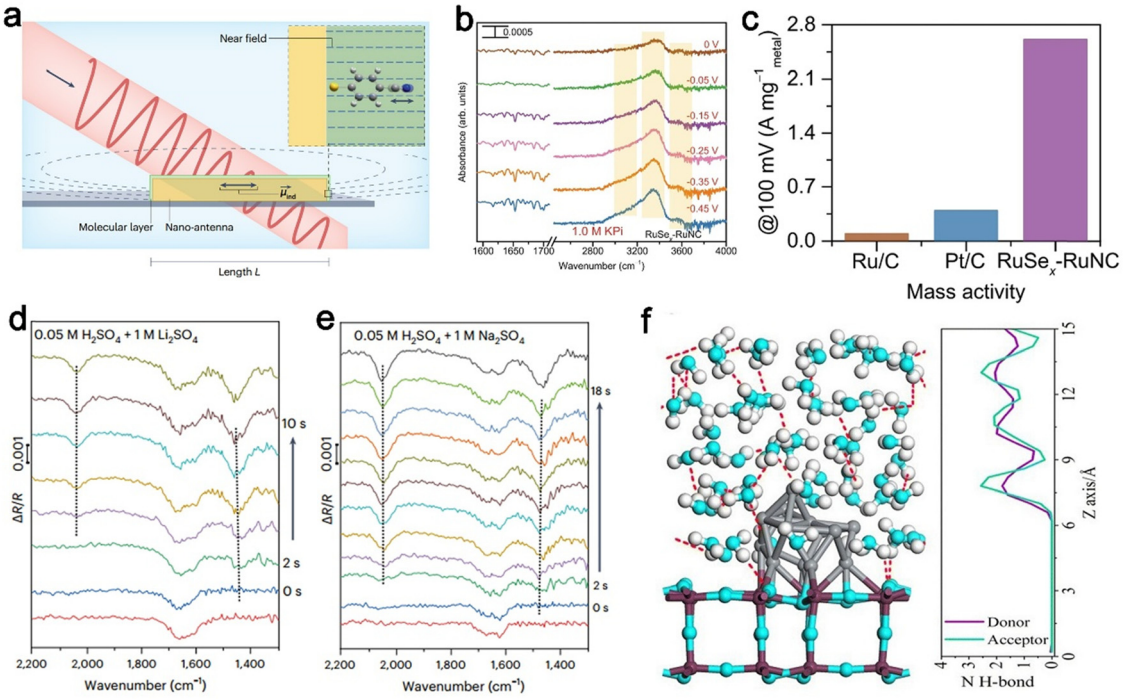

Fig. 8 (a) SEIRAS arises from a localized surface plasmon resonance that is induced into the nano-antenna by the incident IR light.[134] Copyright 2023, Nature Publishing Group. (b) ATR-SEIRAS results of RuSe$_x$–RuNC in neutral media. (c) The mass activity of commercial Ru/C, commercial Pt/C, and RuSe$_x$–RuNC.[16] Copyright 2022, Nature Publishing Group. Time-resolved ATR-SEIRAS of the adsorption process of CO_2 in 0.05 M H_2SO_4 with 1 M Li_2SO_4 (d) and 1 M Na_2SO_4 (e) after the potential was negatively jumped from −0.68 to −0.88 V.[24] Copyright 2024, Nature Publishing Group. (f) Representative snapshots of the interfacial H_2O structures and the corresponding H-bond distributions for Ru/Nb_2O_5.[46] Copyright 2024, Royal Society of Chemistry.

Open Access Article. Published on 01 2568. Downloaded on 4/1/2569 10:24:58.
This article is licensed under a Creative Commons Attribution-NonCommercial 3.0 Unported Licence.

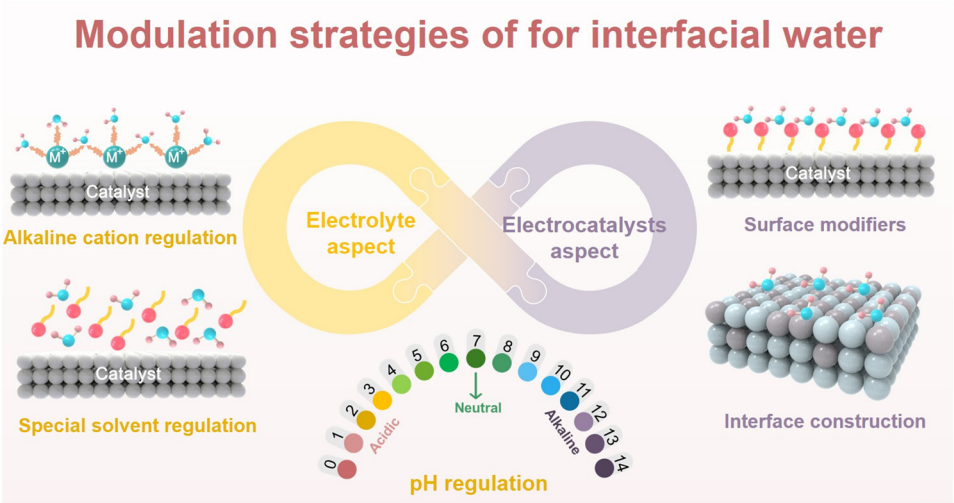

Fig. 9 Summary of modulation strategies of interfacial water for enhanced electrocatalytic performance.

This modulation can direct the electrocatalytic process along a preferred reaction pathway, thereby affecting product distribution, reaction rates and overall selectivity. Although alkali cations are typically inert in aqueous electrochemistry, they exert a profound influence on the chemical and electronic structures of the EDL during electrochemical reactions through various mediating factors. These factors include interfacial water, interactions with reactants, intermediates and products, all of which synergistically enhance the electrocatalytic performance.[151] In this section, the role of alkali cations in modulating the interfacial water's structure to improve the electrocatalytic performance is systematically investigated, with particular emphasis on the underlying reaction mechanisms.

To regulate the size of the cations. Typically, the size of a cation is inversely proportional to its charge density, and the size significantly influences the solvation shell which affects the rate of electrocatalytic reactions. Cations with lower charge densities tend to disrupt the solvation shell more readily at the interface, leading to an increased static dielectric constant to enhance the recombination energy and entropy of H_2O. For example, Huang *et al.* found that larger cations (*e.g.*, Cs^+) are partially desorbed from the negatively charged Pt surface, whereas smaller cations (*e.g.*, Li^+) retain their solvation shells, resulting in slower HER kinetics (Fig. 10a).[38] Similarly, Rao *et al.* found that $RuO_2(110)$ exhibits cation-dependent OER activity with the performance following the trend: $K^+ > Na^+ > Li^+$.[154] Further evidence suggests that larger cations facilitate superior OER performance due to weaker interactions with solvent-shell molecules, thereby reducing interactions between surface OH^- and hydrogen bonds. Based on such findings, Du and colleagues utilized a Li^+ solvent shell to provide an optimal environment for a non-reducing reactor.[155] They found that the energy barrier for the NNH* intermediate formation at −0.3 V (*vs.* RHE) and a pH of 6.8 is only 0.50 eV, significantly lower than the 0.81 eV observed at the pristine Fe–water interface (Fig. 10b). The ammonia synthesis over the Li^+–Fe–water catalyst exhibits a remarkable FE of 29.43%, outperforming Na^+ (25.2%) and K^+ (11.65%) catalysts (Fig. 10c).

Besides, researchers have verified that the interaction between the interfacial water and the size of alkaline cations can partly determine the electrocatalytic performance.[156] Larger cations disrupt the rigidity of the interfacial water's networks, thereby enhancing the reaction kinetics. For instance, Fisher *et al.* demonstrated that larger cations such as Cs^+, K^+ and Na^+ are more effective than Li^+ to break the rigidity of the water networks in alkali metal hydroxide electrolytes. Larger cations lead to the improved accessibility of active sites and enhanced OER performance with a size-dependent trend: Cs^+ (72 mV dec^{-1}) < K^+ (78 mV dec^{-1}) < Na^+ (79 mV dec^{-1}) < Li^+ (96 mV dec^{-1}) (Fig. 10d).[152] A follow-up study found that the size of the cation is the key factor.[24] It was revealed that Li^+ could alter the interfacial water structure more easily than larger cations such as Na^+, K^+, and Cs^+, but fail to lead to the next step of hydrogenation (Fig. 10e). The rigid hydration shell of Li^+ impedes the transfer approach of hydrogen atoms from water to the oxygen in adsorbed CO_2, thereby hindering further hydrogenation. In contrast, larger cations facilitate more flexible water networks, increasing the probability of hydrogen atom transfer to CO_2 and thus enhancing CO_2RR performance (Fig. 10f). This was confirmed by the experimental results of Waegele *et al.* The intermolecular interactions between *CO and interfacial water are disrupted by the action of two larger cations, promoting the hydrogenation of surface-adsorbed carbon monoxide to C_2H_4.[157]

Moreover, larger alkali metal cations also enhance the electrocatalytic activity by buffering the interfacial pH.[158] For instance, water molecules in the hydration shells of larger cations can hydrolyze at the electrode surface, acting as buffers to maintain a lower interfacial pH and higher local CO_2 concentration.[159] The O–H bonds within the hydration shells of larger cations (*e.g.*, Cs^+) are inclined to interact with the negatively charged electrode surface electrostatically, leading to greater polarization relative to smaller cations and consequently higher CO_2RR activity.

 © 2025 The Author(s). Published by the Royal Society of Chemistry

Open Access Article. Published on 01 2568. Downloaded on 4/1/2569 10:24:58.
This article is licensed under a Creative Commons Attribution-NonCommercial 3.0 Unported Licence.

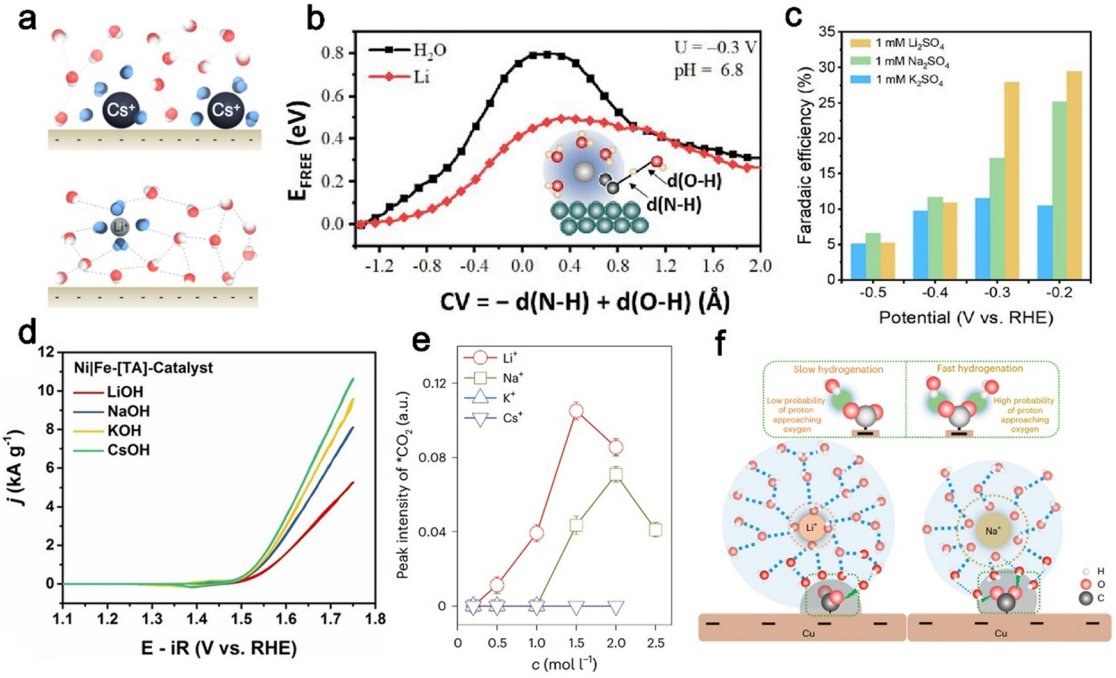

Fig. 10 (a) Schematic illustration of the interactions among interfacial water molecules, cations, and the interface.[38] Copyright 2021, American Chemical Society. (b) E_{FREE} against the CV of the *NNH species formation during c-AIMD simulation with and without Li^+. (c) FE of NH_3 for the Fe NP electrocatalyst in 1 mM Li_2SO_4, Na_2SO_4, and K_2SO_4, respectively.[155] Copyright 2024, American Chemical Society. (d) OER polarization curves of the Ni/Fe–[TA]-catalysts recorded in O_2-saturated 0.1 M LiOH, 0.1 M NaOH, 0.1 M KOH and 0.1 M CsOH electrolytes.[152] Copyright 2022, Wiley-VCH. (e) The dependence of band intensity of adsorbed CO_2 (~1466 cm^{-1}) on cation concentration in 0.05 M H_2SO_4 with Li_2SO_4, Na_2SO_4, K_2SO_4 and Cs_2SO_4. (f) Schematic presentation of the water network around Li^+ and Na^+ and its interactions with adsorbed CO_2.[24] Copyright 2024, Nature Publishing Group.

To adjust the concentration and valence of cations. Another strategy is to increase the concentration and valence of cations, which can significantly influence the structure of interfacial water molecules and the performance of electrocatalytic reactions.[41] In the electrocatalytic process, it was found that the applied overpotential tends to alter the local concentration of cations at the electrode surface. For instance, the HER activity follows the order $K^+ > Na^+ > Li^+$ at low overpotentials in alkaline media containing K^+, Na^+ and Li^+.[160] However, by applying a high potential, the interfacial water structure is drastically altered so that the HER activity in the Li^+-containing electrolyte is much higher than that in the K^+-containing electrolyte (Fig. 11a). Moreover, Hansen *et al.* explored the effect of localized cation concentration on the CO_2RR with an Au–water interface model.[159] The CO_2RR kinetics exhibits the trend: $2K^+ > 1K^+ > 2Li^+ > 1Li^+ > 0AM^+$. Increasing the local cation concentration not only affects the interfacial water's structure and facilitates the activation of CO_2 through short-range interactions between cations and intermediates, while inhibiting the accompanying Volmer reaction in the HER process. This strategy improves the activity and selectivity of the CO_2RR at the Au–water interface.

Further study found that higher valence ions exhibit stronger affinity at the interface, which can influence the behavior of the reacting intermediates.[161] For example, it is possible to optimize the orientation of the interfacial water by adjusting the valence number of the cation to form a downward double "H-down".[162] The water dissociation energies for Li^+, Na^+, K^+, Ca^{2+} and Sr^{2+} systems are 0.30, 0.16, −0.34, −0.29 and −0.38 eV, indicating that higher valence cations significantly affect the interfacial adsorption properties of water molecules. Impressively, the peak frequency of interfacial water increases in the order: $Li^+ < Na^+ < K^+ < Ca^{2+} < Sr^{2+}$, suggesting that cation valence also significantly influences the configuration and hydrogen bonding connectivity of interfacial water molecules. Hence, different types of high valence cations can be customized for different reactions. For example, strongly acidic high-valent cations (*e.g.*, Nd^{3+}) have superior hydrolysis kinetics compared to low-valent cations, while possessing good CO_2 adsorption capacity as well. Thus, a better ability to reduce CO_2 to formic acid is manifested (Fig. 11b).[163] Furthermore, the orientation of interfacial water molecules and their alignment with the interfacial electric field can be reduced to accelerate the Volmer step of the alkaline HER by introducing high-valent and strongly hydrated cations (*e.g.*, Ba^{2+}) (Fig. 11c).[156]

To customize the hydrogen bonding network. Cations tend to interact with interfacial water through a variety of mechanisms, thereby affecting the structure and connectivity of the hydrogen bonding network, which in turn has a significant impact on the activity and selectivity of electrocatalytic reactions.[151] The reaction kinetics and efficiency at the electrode–surface interface are highly correlated with the network structure formed by the ion-water molecules at the interface. For example, Li^+ tends to promote the ordering of the hydrogen bonding network of

Open Access Article. Published on 01 2568. Downloaded on 4/1/2569 10:24:58.
This article is licensed under a Creative Commons Attribution-NonCommercial 3.0 Unported Licence.

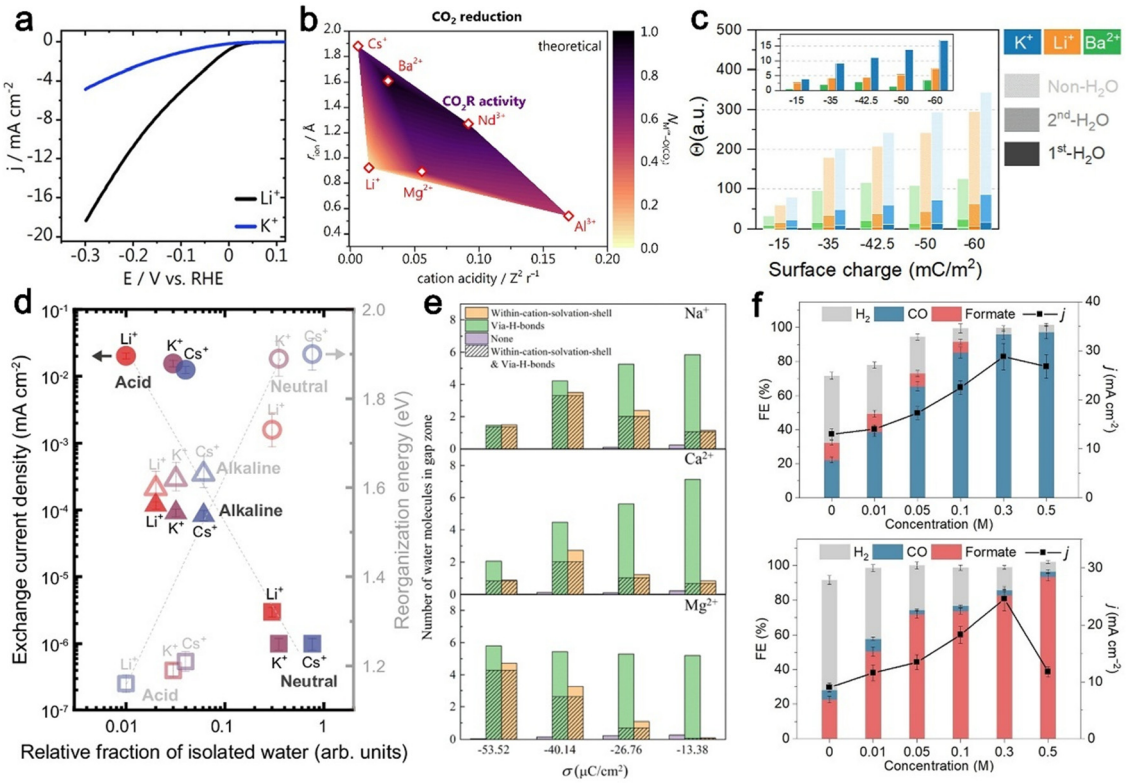

Fig. 11 (a) Hydrogen evolution on stationary electrode platinum in 0.1 M MOH.[160] Copyright 2024, American Chemical Society. (b) CO_2 reduction activity as a potential descriptor with ionic radius and cation acidity.[163] Copyright 2022, American Chemical Society. (c) Absolute net orientation of water along the surface normal.[156] Copyright 2024, American Chemical Society. (d) The reorganization energy of the HER on Au RDE as a function of the relative fraction of isolated water.[137] Copyright 2024, Nature Publishing Groups. (e) The average number of water molecules within the solvation shell of cations and the average number of water molecules interacting with interfacial water molecules *via* H-bonds in the H-bond gap zone of Na^+, Ca^2, and Mg^{2+} systems at different σ.[164] Copyright 2024, Royal Society of Chemistry. (f) Plot of FEs of various products and total current density *vs.* OmimBr concentration in 0.1 M KBr–OmimBr and 0.1 M CsBr–OmimBr at −1.2 V *vs.* RHE.[165] Copyright 2024, Wiley-VCH.

water molecules, while Cs^+ causes the hydrogen bonding network of water molecules to deform significantly, with Li^+ solutions exhibiting higher reaction efficiencies than Cs^+ solutions (Fig. 11d).[137] A recent report confirms that the interaction between the hydration of cations and the interfacial water structure is able to modulate the number of water molecules in the hydrogen bonding gap region and the connectivity of the hydrogen bonding network in EDL. AIMD demonstrates that the cations at the Pt(111)/water interface could modulate the structure and connection of the hydrogen bonding network in the EDL. When the surface charge density becomes more negative, the connectivity of the hydrogen bonding network in the EDL of the Na^+ and Ca^{2+} systems decreases significantly. In contrast, the connectivity of the hydrogen bonding network in the EDL of the Mg^{2+} system increases slightly (Fig. 11e).[164] Further investigations have shown that cation hydration has an important influence on certain reaction pathway choices. The presence of the solvation structure of the different alkali-metal cation can affect the stability of different pathway intermediates.[73] Typically, Han *et al.* converted the product of the CO_2RR from CO (FE_{CO} = 97.3%) to formate ($FE_{Formate}$ = 93.5%) (Fig. 11f).[165] In addition, cations can also optimize the hydrogen bonding network by forming stable coordination structures with the reaction intermediates.[74]

5.1.2. Special solvent regulation. Special solvents, due to their unique physicochemical properties, are able to regulate the properties of interfacial water and thus optimize the electrocatalytic performance precisely.[166] Studies on the modulation of interfacial water by special solvents provide new ideas on the electrocatalysis, especially in the design of efficient electrocatalysts and the optimization of electrocatalytic processes. For reactions such as water splitting and electrooxidation, the selection of appropriate solvents not only enhance the reaction efficiency, but also improve the stability of catalysts.[167,168] In the future, a deeper understanding of solvent effects and interfacial water will provide new ideas for the improvement of electrocatalytic performance and promote the development of clean energy technologies.

To alter the interface microenvironment. Organic solvents can alter the microenvironment at the reaction interface, which in turn affects reactant adsorption and reaction pathways in the electrochemical processes. Grimaud *et al.* utilized a mixture of acetonitrile (ACN) and water as an electrolyte to modulate the hydrophilicity of the electrode/electrolyte interface by varying the supporting salt cations (*e.g.*, TBA^+ and Li^+).[150] It was revealed that Li^+ causes more water to be retained on the

 © 2025 The Author(s). Published by the Royal Society of Chemistry

Open Access Article. Published on 01 2568. Downloaded on 4/1/2569 10:24:58.
This article is licensed under a Creative Commons Attribution-NonCommercial 3.0 Unported Licence.

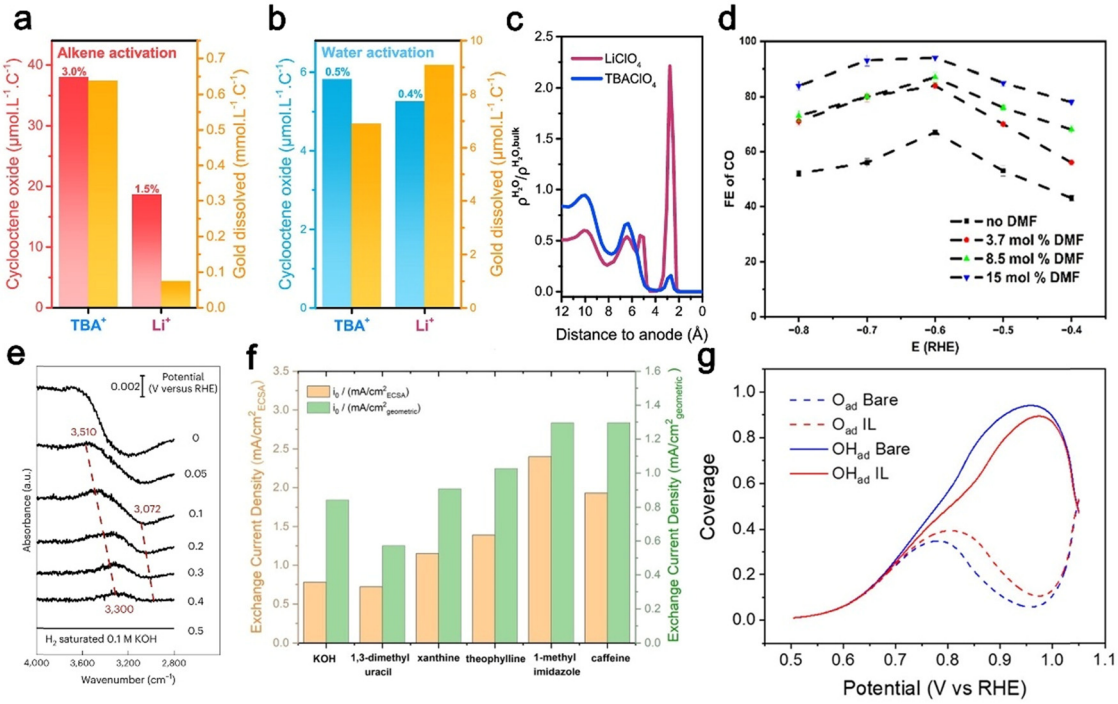

Fig. 12 Corresponding amounts of cyclooctene oxide produced per volume of electrolyte and charge passed and gold dissolved during electrolysis under (a) low overpotential and (b) high overpotential conditions. (c) Density profiles of water at the anode interface in Li^+- and TBA^+-containing electrolytes in the absence of cyclooctene.[150] Copyright 2022, American Chemical Society. (d) Faradaic efficiency of CO formation as a function of potential for different mol% of DMF.[169] Copyright 2023, American Chemical Society. (e) The *in situ* ATR-SEIRAS spectra of interfacial water on a Pt film collected in 0.1 M KOH without 10^{-5} M Me–N_1C_2.[170] Copyright 2023, Nature Publishing Groups. (f) Exchange current densities of the HOR/HER on Pt measured in H_2-saturated 0.1 M KOH and 0.1 M KOH with 0.1 mM organic additives.[171] Copyright 2022, Wiley-VCH. (g) Potential-dependent equilibrium coverages of adsorbed oxygenated species during the ORR.[174] Copyright 2023, American Chemical Society.

electrode surface, which is more favorable to the formation of the Au oxide layer and thus inhibits the dissolution of Au (Fig. 12a and b). The TBA^+ makes the interface more hydrophobic and promotes the reaction between cyclooctene and metallic gold to form more epoxidation products. As a solvent, ACN reduces the overall polarity of the system, while CTAB repels water molecules through the hydrophobic portion of its long chain, forming a hydrophobic interface, which is essential for improving the selectivity of the target reaction (Fig. 12c). As another representative example, it was found that 15 mol% DMF as an electrolyte additive can increase the FE of electrochemical CO_2RR on polycrystalline gold electrodes from 67% to 94% (Fig. 12d).[169] Both the repulsion of interfacial water by the localized hydrophobic environment and the DMF-induced changes in the interfacial water structure contribute to the inhibition of the HER and increase the FE of CO during the CO_2RR.

Solvent additives can also tune the orientation kinetics of the weakly adsorbed water layer. Sun *et al.* found that the introduction of *N*-methylimidazole can facilitate the diffusion of hydroxides across the interface by bringing the second layer of water closer to the platinum surface, thereby promoting the hydrogen evolution and oxidation reaction (HER/HOR) (Fig. 12e).[170] Another example is that the specificized adsorbed organic additives (*i.e.*, theophylline derivatives) favorably promote the dynamic tuning of interfacial water, which disrupts the hydrogen bonding network in the bilayer sufficiently. Thus, the endowed HOR/HER activity in polycrystalline Pt bases is increased by threefold (Fig. 12f).[171] As electrolytes or solvents, the effect of ionic liquids on the interfacial water behavior has been widely studied in the field of electrocatalysis.[172,173] For instance, the hydrophobic bis-perfluoroalkyl sulfonimides optimizes the interaction between the catalyst surface and interfacial water and reduces the concentration of water at the metal/electrolyte interface, which in turn reduces the solvation of the adsorbed species and prevents the formation of an ordered hydrogen bonding network. Namely, the barrier to the final step of the ORR mechanism is lowered by reducing the solubility of the active OH_{ad} and weakening its interaction with the catalyst surface (Fig. 12g).[174] With a deeper understanding of the ionic liquid regulatory mechanism, its application in electrocatalysis could be more promising.

To modulate the proton-coupled electron transfer process. The connection of interfacial water to the proton-coupled electron transfer (PCET) process plays a crucial role in electrocatalytic reactions.[36] Organic solvents will modulate the interfacial water to alter electrocatalytic reaction paths, rates, and selectivity through hydrogen bonding network, solvation effects, *etc.* For instance, Zhang *et al.* proposed a molecular engineering strategy to modulate the water activation with high Guttmann donor numbers as solvated shell modulators.[167] In a model electrolyte with 5 M DMSO as an additive, the selectivity of CO for Ag foil is

Open Access Article. Published on 01 2568. Downloaded on 4/1/2569 10:24:58.
This article is licensed under a Creative Commons Attribution-NonCommercial 3.0 Unported Licence.

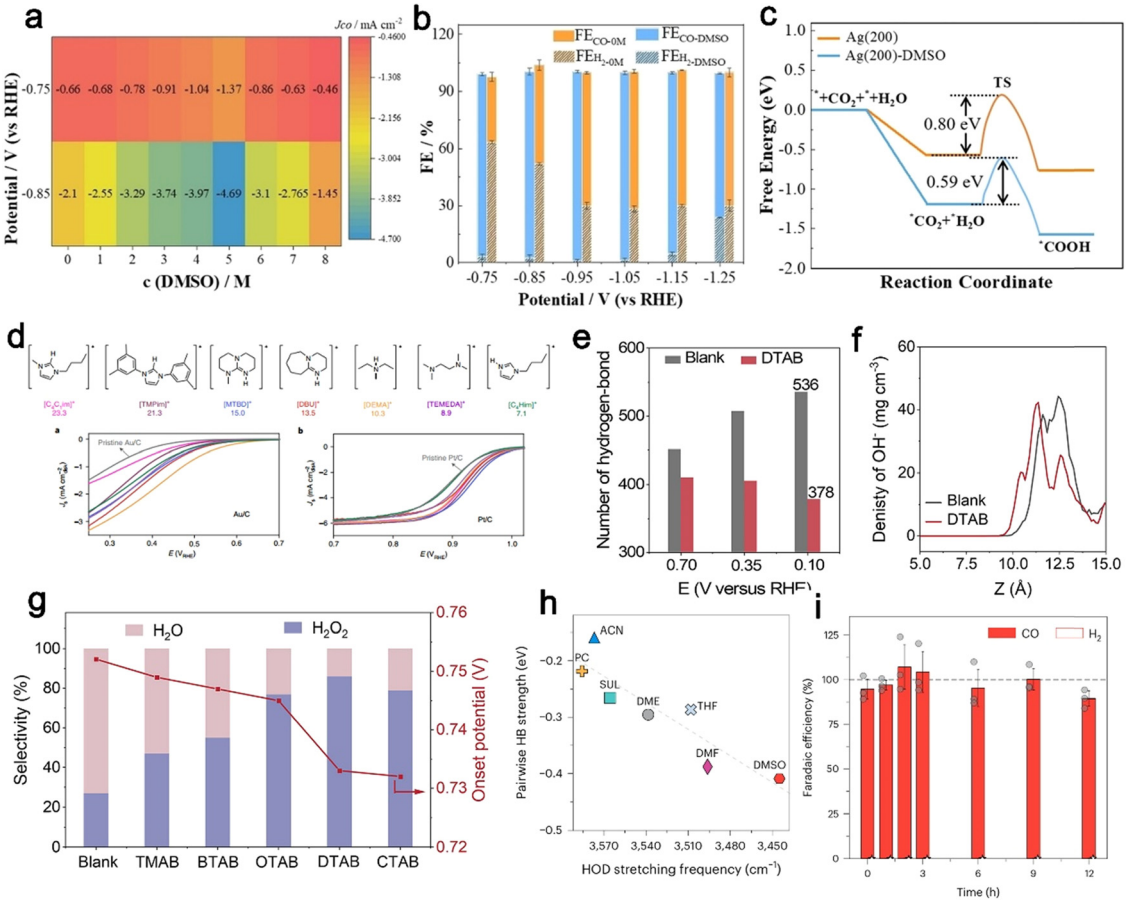

Fig. 13 (a) Heatmaps of CO partial current density at −0.75 V and −0.85 V in KCl–DMSO-*x* electrolyte. FE in (b) CO_2-saturated 0.5 M KCl and KCl–DMSO-5. (c) Energy barriers of transitional state formation for $*CO_2$ to *COOH conversion with and without DMSO additive.[167] Copyright 2023, Wiley-VCH. (d) The ORR activity on ionic-liquid-modified Au/C and Pt/C measured in O_2-saturated 0.1 M $HClO_4$.[36] Copyright 2021, Nature Publishing Groups. (e) Number of hydrogen bonds in KOH and DTAB-modified KOH electrolyte at 0.10 V_{RHE}. (f) Radial density distribution of OH^- in KOH and DTAB-modified KOH electrolyte at 0.10 V_{RHE}. (g) The H_2O_2 selectivity and onset potential at 0.3 V_{RHE} in KOH electrolytes.[166] Copyright 2024, American Chemical Society. (h) The pairwise HB strength from DFT calculations and the HOD stretching frequency extracted for 1 M water in different solvents. (i) Product distribution analysis for DMSO solution using a zinc electrode at −10 mA cm^{-2} over 12 h electrolysis.[175] Copyright 2024, Nature Publishing Groups.

increased up to 99.2%, with FE_{CO} higher than 90.0% in the range of −0.75 to −1.15 V (V *vs.* RHE) (Fig. 13a and b). Impressively, the organic molecules occupy the first solvation layer of K^+ and accumulate in the electric double layer, reducing the H_2O density and the relative content of proton donors at the interface and inhibiting the HER. Adsorbed H_2O is stabilized by the second sphere effect, and the weakening of the O–H bond promotes its dissociation, accelerating the subsequent kinetics of the protonation of $*CO_2$ and lowering the energy barrier (Fig. 13c). Similarly, Shao *et al.* varied the localized proton activity by a series of protonated ionic liquids in the interfacial layer of Pt and Au, where the intrinsic ORR activity forms a volcano-shaped correlation with the pK_a of the ionic liquids.[36] Enhanced ORR activity is attributed to the enhanced hydrogen bonds between the ORR product and ionic liquids with similar pK_a (Fig. 13d).

The modulation of the PCET process will also directly convert the electrocatalytic pathway. Some researches reveal that surfactants modulate the interfacial water structure to influence the PCET process and thus change the reaction path. When hydrophobic quaternary ammonium cationic surfactants are introduced into the electrolyte, a stable hydrophobic interface is formed, which effectively disrupts the interfacial hydrogen bonding network and hinders the proton transfer. Hence, the limited proton supply at the reaction interface drives the ORR to follow the two-electron pathway with fewer protons involved (Fig. 13e).[166] Noteworthy, the insufficient supply of protons leads to the accumulation of OH^-, which causes a local pH elevation and greatly improves the selectivity of the two-electron ORR to generate H_2O_2 (Fig. 13f and g). One more example, a study systematically investigated the effects of different non-aqueous solvents interacting with water molecules on the hydrogen bonding network strength and kinetics of water.[175] It turns out that the electron-donating capacity (donor number) of solvents can well describe the hydrogen bonding network strength of water, and is linearly correlated with the HER activity (Fig. 13h). Utilizing the solvent to modulate the hydrogen bonding network of water molecules, CO_2

 © 2025 The Author(s). Published by the Royal Society of Chemistry

Open Access Article. Published on 01 2568. Downloaded on 4/1/2569 10:24:58.
This article is licensed under a Creative Commons Attribution-NonCommercial 3.0 Unported Licence.

can be reduced to CO with high selectivity, and the side reaction of the HER is almost completely suppressed. In acidic medium, high donor number solvents (*e.g.*, DMSO) inhibit the proton reduction and obtain nearly 100% CO_2 reduction selectivity without carbonate loss for a long time (Fig. 13i).

5.1.3. pH regulation. Changes in pH can affect the arrangement of water molecules at the interface and the hydrogen bonding network significantly. To some degree, the pH effect determines the difference in the kinetics of the HER under acidic and alkaline conditions. Subbaraman *et al.* attributes the slower reaction rate in alkaline media to the more challenging Volmer step ($H_2O + e^- \rightarrow {}^*H + OH^-$) compared to the acidic environment ($H_3O^+ + e^- \rightarrow {}^*H + H_2O$).[176] Subsequently, Kopper *et al.* introduces the theory of the potential of zero free charge (pzfc) to explain the differences in HER dynamics between acidic and alkaline media. They argue that in acidic media, where the pzfc is closer to the HER region, the recombination energy of interfacial water associated with proton transport through the bilayer is smaller, thereby facilitating HER dynamics.[35] However, the pzfc theory fails to fully explain the HER kinetics at high pH, and their recent study attributes the increase in HER activity at higher pH to an increase in the local cation concentration, which stabilizes the transition state of the rate-determining Volmer step through good interactions with dissociated water molecules.[177] In contrast, Jung *et al.* attributes the higher activity in high-pH electrolytes to the localized generation of H_3O^+ intermediates, which can create a unique acid-like local reaction environment on the catalyst surface to lower the energy barrier for the overall reaction.[178]

In addition to the HER, the pH effect profoundly affects the nature of interfacial water in other electrocatalytic reactions. For example, the strong electric field polarizes interfacial water molecules around metal centers into an "O-down" conformation, disrupting hydrogen bonds between oxygenated intermediates and interfacial water. This result hinders the proton transfer and slows the reaction kinetics, confirming that the pH dependence of ORR activity on FeCo–N_6–C catalysts is driven by the differences in PCET reaction kinetics induced by interfacial water orientation and hydrogen bonds.[179] Similarly, the attenuation of Bi-based catalyst performance in acidic CO_2RR is attributed to a shift in local pH from neutral to acidic as well. Such pH changes result from the decreased K–H_2O due to competitive adsorption between K^+ and protons.[180]

5.2. Electrocatalyst aspect

Although electrocatalyst design has long represented a separate segment in electrocatalysis, recent studies have found that the surface state of the electrocatalyst or electrode has an important influence on the structure and properties of interfacial water.[64,67] For example, adjusting the electrocatalyst's oxyphilicity, hydrophilicity, or local electric field can profoundly affect the local density of water molecules, interfacial hydrogen bonding arrangements and water molecular dynamics, which in turn affects the activity and selectivity.[181–183] In this section, the modulation of interfacial water from both the points of surface modification and interfacial construction of electrocatalysts is summarized and the intrinsic mechanisms are analyzed.

5.2.1. Surface modifiers. The role of electrocatalyst surface modifiers in electrocatalytic reactions is multifaceted, especially in regulating the behavior of water at the electrocatalysis interface. Surface modification of electrocatalysts can affect the adsorption and dissociation of water molecules on the surface of electrocatalysts, as well as the interaction with reactants and products through changing the chemical environment and optimizing reaction pathways.[184–187] In the following section, we categorize surfactants and organic additives, detailing the mechanisms behind the tuning of interfacial water behavior to enhance the electrocatalytic performance.

Surfactants. Surfactants tend to modulate the interfacial water's environment in the vicinity of the electrocatalyst to achieve enhanced electrocatalytic performance. Typically, quaternary ammonium cationic surfactants such as cetyltrimethylammonium bromide (CTAB), have been widely applied to fine-tune the selectivity of the CO_2RR and organic-electrolytic synthesis *via* water management.[163,188] For instance, Li *et al.* combined quaternary ammonium cationic surfactants as electrolyte additives and found that the surfactants act as modifiers of interfacial water to improve the environment by repelling isolated water and inhibiting the orientation of water to ordered structures. This strategy promotes CO_2 enrichment at the charged interfaces to increase the selectivity of CO_2 electroreduction to CO.[77] Similarly, Sun *et al.* successfully prepared an artificial electrode/electrolyte interface by coating the electrode surface with a $R4N^+$ surfactant (Fig. 14a).[187] This artificial electrode/electrolyte interface has high CO_2 permeability, which facilitates CO_2 transport and hydrogenation (Fig. 14b). Due to unique interactions between anions and water molecules, Li *et al.* explored the reaction mechanism of the CO_2RR by adding anionic surfactants to various electrolytes, including sodium dodecyl sulfate (SDS).[189] This result shows that anionic surfactants fail to adsorb on the electrode surface but affect the aqueous environment near the electrode surface (Fig. 14c). The increase of CO selectivity is attributed to the enhancement of the hydrogen bonding network, which can reduce the dissociative activity of the water and thus facilitate the proton coupling pathway of the CO_2RR (Fig. 14d).

Surfactants can modulate the enrichment of interfacial water on the surface of the catalyst.[190,191] Li and colleagues reported that the modulation of interfacial hydrophobicity using a quaternary ammonium cationic surfactant inhibits the HER and promotes alkynyl alcohol hemihydrogenation.[8] As another representative example, by incorporating a small amount of counter-charged anionic polymers (*e.g.*, PFSA) into the cationic covalent organic skeleton (cCOF) on the electrocatalyst surface, the hidden positive charge inside the cCOF can be effectively released to prevent the outward migration of OH^- and inward migration of cations generated *in situ* on the electrocatalyst surface.[186] *In situ* characterization and theoretical calculations demonstrate that the cCOF/PFSA electrocatalyst forms a hydrophobic and strongly alkaline microenvironment, which enables the adsorption strength and conformation of the *CO intermediate to be optimized.

Open Access Article. Published on 01 2568. Downloaded on 4/1/2569 10:24:58.
This article is licensed under a Creative Commons Attribution-NonCommercial 3.0 Unported Licence.

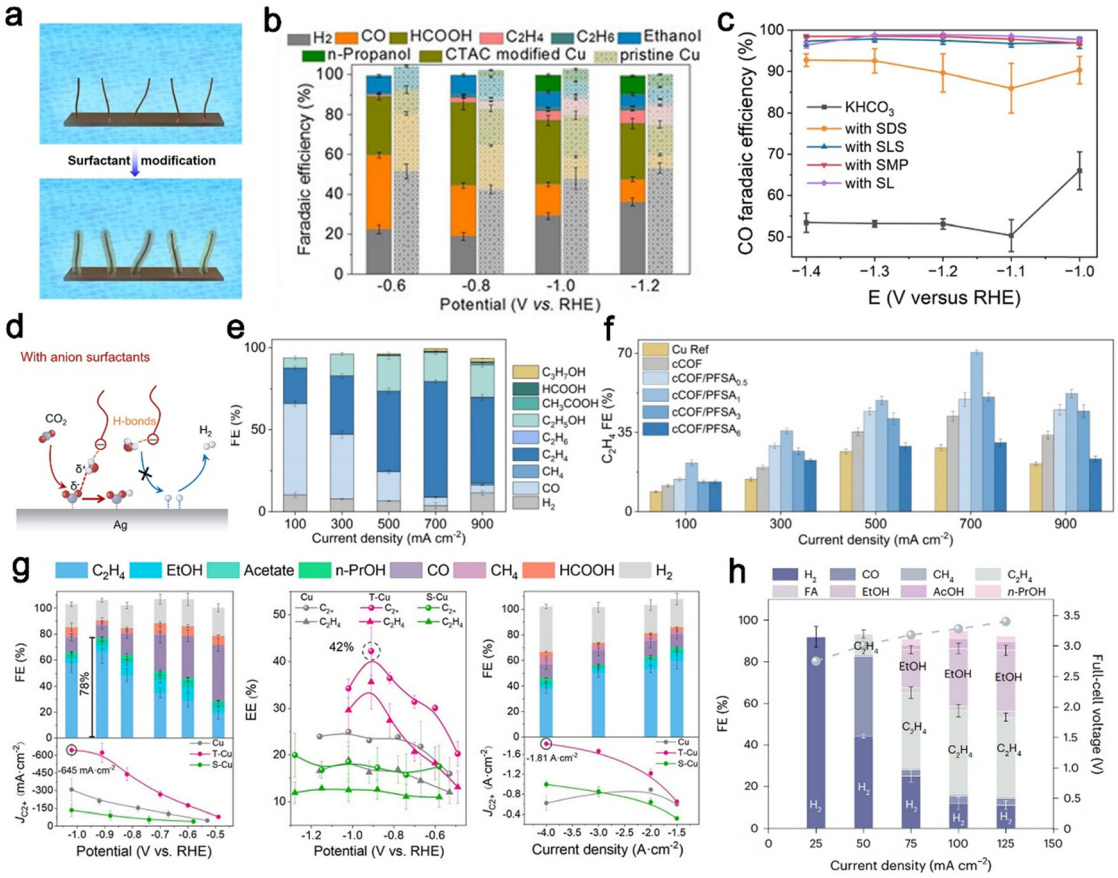

Fig. 14 (a) Schematic of a Cu NW array and Cu NW array after surfactant modification. (b) Faradaic efficiencies at various potentials of the Cu NW electrodes with and without CTAC.[187] Copyright 2020, Wiley-VCH. (c) CO faradaic efficiency of different electrolyte systems. (d) Schematic diagram of the catalytic pathway after the introduction of anionic surfactants.[189] Copyright 2024, American Chemical Society. (e) FEs of various products on the cCOF/PFSA$_1$ catalyst during the CO_2RR. (f) C_2H_4 FEs of various catalysts at different current densities.[186] Copyright 2024, American Chemical Society. (g) Product distributions on T–Cu and current densities of C_2^+ products on Cu, T–Cu, and S–Cu from −0.49 to −1.02 V, energy efficiency of C_2H_4 and C_2^+ products for those catalysts and product distributions on T–Cu and current densities of C_2^+ products on Cu, T–Cu and S–Cu from −1.5 to −4 A cm^{-2}.[192] Copyright 2023, Wiley-VCH. (h) Full-cell-voltage performance in a slim flow cell from 25 mA cm^{-2} to 125 mA cm^{-2}.[193] Copyright 2023, Nature Publishing Groups.

Impressively, the cCOF/PFSA achieves a 70.5% faradaic efficiency of C_2H_4, with a fractional current density in excess of 470 mA cm^{-2} (Fig. 14e and f).

Organic additives. The utilization of organic additives to modify the electrocatalyst surface to enhance the electrocatalytic performance has been widely reported. Zheng *et al.* reported the fine-tuning of interfacial water by surface assembly of toluene on Cu nanosheets, resulting in an enhanced performance of faradaic efficiency of 78% for C_2^+, a partial current density of 1.81 A cm^{-2} and an energy efficiency of 42% compared to bare Cu and long-chain alkyl-modified Cu with predominantly CO products (Fig. 14g).[192] The surface toluene functionalization of electrocatalysts delays the transfer of water to the electrocatalyst surface, which allow both a high CO_2 ratio and a suitable hydrogen content to facilitate the conversion of CO_2 to C_2^+. Besides, Sargent *et al.* adopted immobilized cationic group modification to improve the C_2^+ selectivity and stability of electrocatalysts in the strongly acidic environments.[193] The electrolyte alkali metal cations are replaced by integrating a thin layer of ionic cross-linked polymer with immobilized cationic functional groups on the Cu surface. The water management properties of this layer of polymer minimizes proton migration and allows operation at a moderate voltage of 3.3 V and a weakly basic local pH with a C_2^+ faradaic efficiency of 80 ± 3% (Fig. 14h).

Ionic liquids are ideal for modulating interfacial water properties due to their adjustable polarity, high ionic conductivity and wide electrochemical window.[194,195] Snyder *et al.* demonstrated that the ionic liquid films reduce the water content at the interface and hinder the formation of hydrogen bonding networks. The diminished solvation of the active OH_{ad} species attenuates its interaction with the electrocatalyst surface, thereby lowering the energetic barrier for the final step in the ORR.[175] Recently, an investigation revealed that the ionic liquid modification can inhibit the formation of inactive carboxylate species by improving the hydrogen bonding network of interfacial water, leading to efficient CO_2RR performance.[166] It was found that water concentrations up to 0.5 M can trigger no significant faradaic reaction when CO_2 is trapped between

 © 2025 The Author(s). Published by the Royal Society of Chemistry

Open Access Article. Published on 01 2568. Downloaded on 4/1/2569 10:24:58.
This article is licensed under a Creative Commons Attribution-NonCommercial 3.0 Unported Licence.

the [EMIM]$^+$ ring and the electrode surface. Such findings refute the idea that the interfacial water serves as a source of free protons, and that the interfacial water merely acts as a hydrogen bonding donor. Furthermore, alcohols of different acidity levels can modulate the hydrogen bonding network in the interfacial microenvironment, thereby reducing the energy required for the CO_2RR.

5.2.2. Interfacial construction. The field of interfacial water in electrocatalysis provides insight into the design of electrocatalysts. Through effective interfacial construction strategies, properties such as interfacial water arrangement, hydrogen bonding network, and structural dynamics can be optimized to promote efficient and stable electrocatalytic systems. Therefore, interfacial design is of great importance in the modulation of interfacial water and may be a key direction in electrocatalyst development in the future. In this section, we summarize three strategies for modulating interfacial water by interfacial construction at the electrocatalyst level, including construction of built-in interfacial electric fields, optimization of interfacial hydrogen bonds, and regulation of the active sites (Fig. 15).

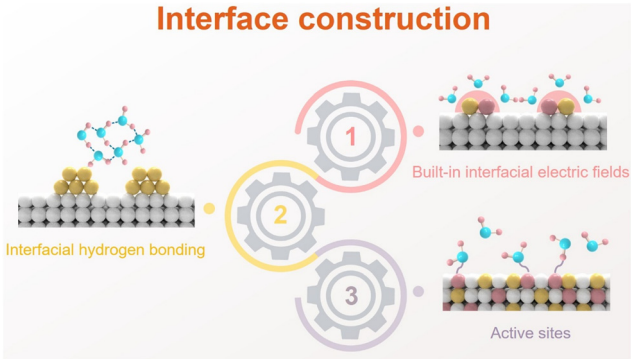

Fig. 15 Schematic illustration of interfacial construction.

To construct built-in interfacial electric fields. Electrocatalysis inherently involves the driving of reactions under the influence of an external electric field. However, the built-in electric field, generated by the electrocatalyst's electronic structure, interfacial effects, or material defects, operates independently of any external electric field. A built-in electric field can optimize the adsorption behavior of water molecules and modulates the dynamics of interfacial water during the electrocatalysis, ultimately enhancing the electrocatalytic performance. In heterogeneous catalysts, interfacial effects between different components often give rise to strong built-in electric fields. For instance, Mu *et al.* developed $Ni(OH)_2/Cu(OH)_2$ heterojunctions on copper foam using a wet-chemical method (Fig. 16a and b).[183] The built-in electric field between $Ni(OH)_2$ and $Cu(OH)_2$ directs electron flow from $Cu(OH)_2$ to $Ni(OH)_2$, inducing an inhomogeneous distribution of valence charge at the Ni interface. The directed electron flow disrupts the arrangement of interfacial water, which can weaken hydrogen bonding connectivity and enhance mass transfer at the interface of the heterostructure (Fig. 16c). Following a similar strategy, Zhang and colleagues designed a nanostructure encapsulating Ni_3N nanoparticles ($Ni_3N@W_5N_4$) in an ultrathin W_5N_4 shell (1–5 nm thick) (Fig. 16d).[196] The electric field at the nitride interface facilitates the electron transfer from W_5N_4 to Ni_3N, optimizing the electronic structure of the W_5N_4 shell. The localized electric field near the interface induces strong valence changes in W atoms, lowering the energy barrier of water dissociation from 1.40 eV to 0.26 eV (Fig. 16e). Besides, Luo *et al.* designed Ru/Nb_2O_5 heterojunction electrocatalysts under the guidance of AIMD calculations.[46] Impressively, the Nb_2O_5 allows the transport of H_2O/OH^* by disrupting the hydrogen bonding network in the interfacial region, which increases the content of free water near Ru and accordingly enhances the HER activity under neutral conditions (Fig. 16f). Among various electrocatalysts, Ce-based electrocatalysts have attracted much attention due to their remarkable electron transfer properties and strong valence-changing abilities. For example, porous $Ni(OH)_2$–CeO_x heterostructures containing an optimal Ce ratio, exhibit excellent HER performance in alkaline seawater, requiring only 148 mV overpotential at 100 mA cm^{-2} (Fig. 16g).[197] Analogously, the $NiSe_2$–$Ce_2(CO_3)_2O$ heterostructure optimizes the coordination environment, facilitates the dynamic reconfiguration of catalytical active sites, and reduces the water dissociation energy, which significantly enhance the electrocatalytic activity.[198]

In addition to heterogeneous structures, several studies have also reported other methods for inducing interfacial electric fields. Liu *et al.* proposed the design of Ir/Ru double-coupled single-atom sites to generate asymmetrical localized electric fields, which modulates the H_2O adsorption configuration and orientation, yielding an electric field strength of 4.00×10^{10} N/C.[199] The IrRu DSACs facilitate an asymmetric "H-down" adsorbed H_2O configuration, increasing the H–O–H bond angle and promoting interfacial water dissociation (Fig. 16h). This strategy realizes an overpotential of only 10 mV at a current density of 10 mA cm^{-2} (Fig. 16i). Furthermore, Han *et al.* introduced an "*in situ* disruption and neighbor compensation" strategy to optimize the hydrogen bonding network of interfacial water. Theoretical simulations affirm that the local concentration of hydrated K^+ at the electrocatalyst surface optimizes the water dynamics and intermediate adsorption (Fig. 16j).[200] Besides, a recent strategy proposed by Chen *et al.* adopted the topological morphology manipulation to enhance the activity of electrocatalysts.[201] By anchoring FeO_x clusters on $Co_{0.75}Fe_{0.25}P$ phosphide nanorods, surface electric field enhancement and topology-induced interfacial electric fields were utilized to optimize the reactant adsorption. These enhancements promote the adsorption of polar H_2O/OH^- and facilitate the desorption of H_2/O_2, thereby improving the electrocatalytic performance.

To optimize interfacial hydrogen bonds. Interfacial hydrogen bonds play a crucial role in determining the adsorption behavior of water molecules on the electrocatalyst surface, which can affect their configuration and binding strength to enhance the proton transport and electrocatalytic activity. For example, Ren *et al.* modulated the interfacial water networks with M–O atom pairs, and the electron-rich environment of the O atoms shifts the water molecule configuration from "O-down" to

Open Access Article. Published on 01 2568. Downloaded on 4/1/2569 10:24:58.
This article is licensed under a Creative Commons Attribution-NonCommercial 3.0 Unported Licence.

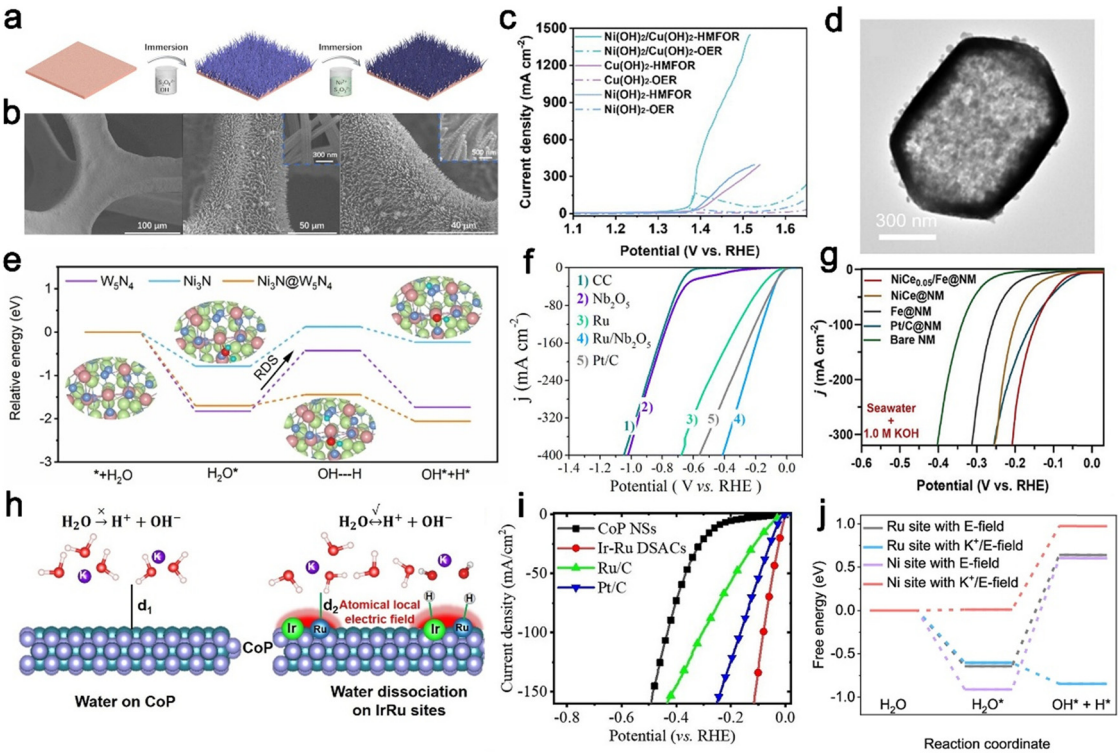

Fig. 16 (a) Schematic representation of the synthesis of the $Ni(OH)_2/Cu(OH)_2$ heterostructure. (b) SEM images of the Cu foam, $Cu(OH)_2$ and the $Ni(OH)_2/Cu(OH)_2$ heterostructure. (c) Polarization curves of $Ni(OH)_2/Cu(OH)_2$, $Ni(OH)_2$ and $Cu(OH)_2$ in 1 M KOH with and without 50 mM HMF.[183] Copyright 2024, Royal Society of Chemistry. (d) TEM images of $Ni_3N@W_5N_4$. (e) H_2O dissociation energies on W_5N_4, Ni_3N, and $Ni_3N@W_5N_4$.[196] Copyright 2024, Wiley-VCH. (f) LSV curves of CC, Nb_2O_5, Ru, Ru/Nb_2O_5, and 20% Pt/C tested in 1.0 M PBS.[46] Copyright 2024, Royal Society of Chemistry. (g) LSV polarization curves toward the HER in 1.0 M KOH.[197] Copyright 2024, Wiley-VCH. (h) Schematic of interface H_2O reorientation induced by atomic electric field. (i) Electrochemical polarization curves of the as-prepared catalysts.[180] Copyright 2023, Wiley-VCH. (j) Free energy diagrams of H_2O adsorption/dissociation on different sites without K^+ and with K^+.[200] Copyright 2024, Nature Publishing Group.

"H-down".[37] The interfacial water networks become more disordered, thereby enhancing the flexibility of the water layer and improving proton transport. The optimized Rh, O-$MoSe_2$ shows excellent HER performance in both acidic and alkaline electrolytes (Fig. 17a and b). Hydrogen shuttling and exchange within the network were also found to be critical to optimizing the performance.[202] Analogously, Zhai *et al.* covered the surface of Mn-doped Co_3O_4 with a nitrogen-doped carbon layer, in which CN units act as hydrophilic centers to modulate the hydrogen bonding network and activate water molecules for the OER.[203] Remarkably, Mn-doped Co_3O_4@CN achieves an overpotential of 395 mV at 10 mA cm^{-2}. Furthermore, adjusting the binding energy of hydroxyl intermediates could regulate the interfacial water's configuration.[204] The introduction of the oxyphilic Cr and W can modulate the orbital occupancy of Ru and promote the adsorption of hydroxyls, leading to the great HOR performance in alkaline media (Fig. 17c). Recently, a pioneering study achieved delamination by replacing WO_4^{2-} with OH^- and H_2O through the introduction of high oxidation state sacrificial elements and cation exchange strategies (Fig. 17d).[205] The formed CWO-del-48 stabilizes water and hydroxyl species by affecting the hydrogen bonding network of water molecules, thereby reducing the solubility of Co ions in acids and improving stability (Fig. 17e).

To regulate the active sites for interfacial water. By regulating the distribution of active sites, it is possible to optimize the reaction path and electrocatalytic activity. For example, atomic-level doping can effectively modulate the electronic structure of electrocatalysts and adjust the adsorption strength of water molecules. Typically, Li *et al.* prepared a series of Cu-doped SnO_2 electrocatalysts with a simple co-precipitation method, in which Cu doping reduces the oxidation state of Sn and induces a distorted structure with stabilized Sn–O species as compared to crystalline SnO_2 (Fig. 18a).[206] This strategy can weaken the water adsorption on the Sn sites and enhance the dissociation of interfacial water, which effectively suppresses the competing HER and facilitates the hydrogenation of $*CO_2$ to *OCHO (Fig. 18b). Notably, the FE of formate over the optimized Cu-doped SnO_2 electrocatalysts reaches an outstanding level (~91%) (Fig. 18c). Likewise, Liu *et al.* constructed phosphorus-doped In_2O_3 nanosheets (Fig. 18d), which exhibit good CO_2RR performance with a faradaic efficiency of 92.1% for formate and a partial current density of 200 mA cm^{-2} (Fig. 18e).[207] The $(P–O)^{\delta-}$ species on the surface of the OD-PIn is able to promote the adsorption of water and dissociation to release H^+. Meanwhile, changes in the electronic structure of the In active center enhances the adsorption of carbon dioxide, and these two factors simultaneously promote the formation of formate

 © 2025 The Author(s). Published by the Royal Society of Chemistry

Open Access Article. Published on 01 2568. Downloaded on 4/1/2569 10:24:58.
This article is licensed under a Creative Commons Attribution-NonCommercial 3.0 Unported Licence.

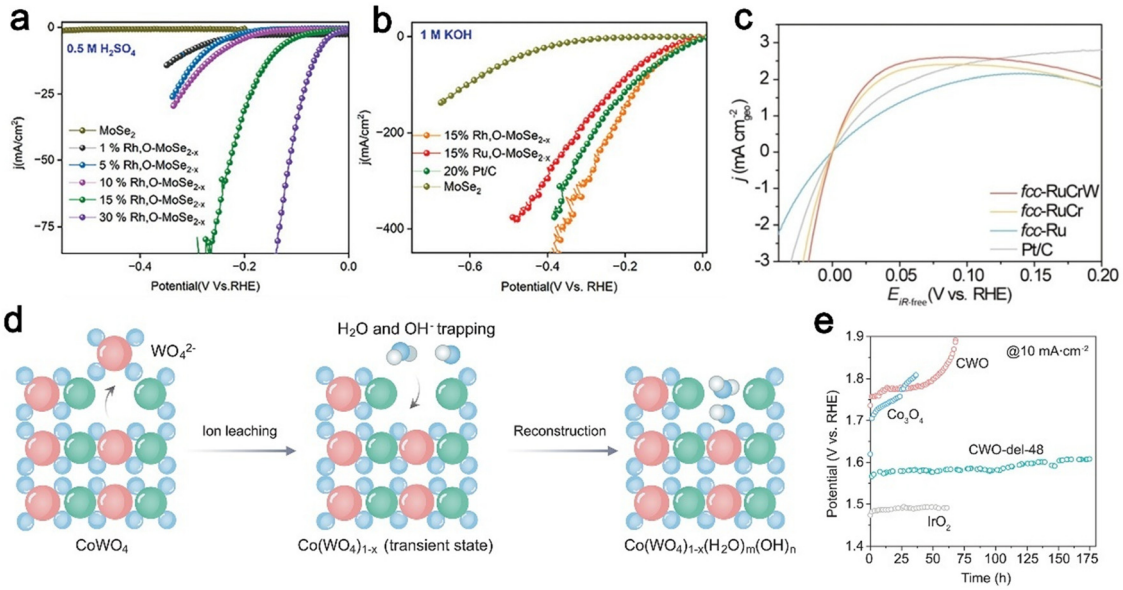

Fig. 17 HER polarization curves in (a) 0.5 M H_2SO_4 and (b) 1 M KOH.[37] Copyright 2024, Wiley-VCH. (c) HOR polarization curves of the fcc-Ru, fcc-RuCr, fcc-RuCrW, and commercial Pt/C in H_2-saturated 0.1 M KOH.[204] Copyright 2024, Copyright 2024, Wiley-VCH. (d) The process and crystallographic representation of CWO delamination into CWO-del-48 through base treatment. (e) Chronopotentiometry stability tests in 0.5 M H_2SO_4 electrolyte at constant 10 mA cm^{-2}.[205] Copyright 2024, American Association for the Advancement of Science.

(Fig. 18f and g). Qiao *et al.* found that Cu modification in Cu/Mo_2C can not only regulate the d-band center of Mo_2C and attenuate the strong adsorption of H* at Mo sites, but also has the functions of activating water molecules and optimizing the interfacial water structure.[208] Encouragingly, Cu/Mo_2C achieves an excellent HER performance, realizing an overpotential of only 24 mV at a current density of 10 mA cm^{-2}. By introducing surface defects, the increased active sites not only affect the electronic structure of electrocatalysts, but also modulate the behavior of interfacial water molecules, which in turn affects the electrocatalytic performance.[209] For instance, Liu *et al.* prepared CeO_2@$CoSe_2$ nanoneedles on carbon cloth by a hydrothermal

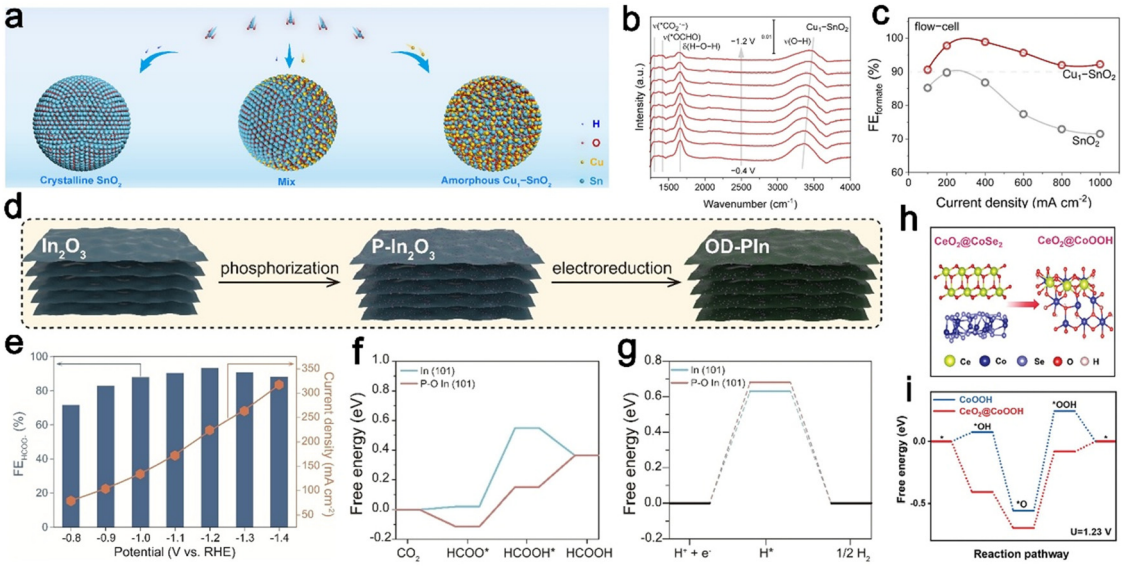

Fig. 18 (a) Schematic diagram for the preparation of SnO_2 and Cu_x–SnO_2 catalysts. (b) *In situ* ATR-FTIR spectra of Cu_1–SnO_2 under applied potentials from −0.4 to −1.2 V in CO_2-saturated 0.1 M $KHCO_3$. (c) $FE_{formate}$ at applied current densities on the SnO_2 and Cu_1–SnO_2 in 1 M KOH with a flow cell.[206] Copyright 2024, American Chemical Society. (d) Schematic illustration showing electrochemical reduction of P-In_2O_3 to OD-PIn under operando CO_2RR conditions. (e) FE and j_{total} of OD-PIn. ΔG diagrams for (f) CO_2RR to HCOOH and (g) the HER on In(101) and P–O In(101) surfaces.[207] Copyright 2024, Wiley-VCH. (h) Schematic diagram of surface reconstruction from CeO_2@$CoSe_2$ into CeO_2@CoOOH. (i) Gibbs free energy diagrams of CoOOH and CeO_2@CoOOH at U = 1.23 V.[209] Copyright 2024, Wiley-VCH.

Open Access Article. Published on 01 2568. Downloaded on 4/1/2569 10:24:58.
This article is licensed under a Creative Commons Attribution-NonCommercial 3.0 Unported Licence.

method.[209] Further analysis reveals that CeO_2 contains abundant O vacancies, which can facilitate OH^- adsorption and promote the reconfiguration of $CoSe_2$ to CoOOH at lower potentials (Fig. 18h and i). Remarkably, CeO_2@$CoSe_2$/CC exhibits good OER activity with an OER overpotential of 245 mV at 10 mA cm^{-2} due to CeO_2-promoted H_2O dissociation and H* adsorption on $CoSe_2$.

Other strategies. In addition to the above three modulation strategies, local strain engineering is another additional avenue for facilitating the behavioral transition of interfacial water. Lattice strain induces changes in atomic spacing, which affects the overlapping distribution of electronic energy bands.[210,211] In particular, the d-band centers of transition metal compounds are affected by strain, leading to modulated electrochemical behavior.[212] The thermodynamic energy of adsorption of polyatomic molecules (*e.g.*, H_2O, CO_2, N_2, NH_3, *etc.*) can be tuned on strain solid surfaces.[213] For example, Fan *et al.* demonstrated that biaxial strain could effectively induce the transformation of K^+–H_2O into tetrahedral coordinated water.[66] Biaxial strain can effectively stabilize the OH* on the $MoSe_2$ surface and change the water adsorption conformation from "O-down" on Mo to O^- level on OH* through stronger hydrogen bonds, thus promoting the intrinsic HER activity. Furthermore, Li *et al.*'s work demonstrated the modulation of interfacial water, intermediates and electrocatalytic activity by tuning valence states. During the HER process, high valence Ru (n^+) surfaces have more moderate adsorption energies for interfacial water, H* and HO*, which can promote the performance of the basic HER.[15] It is also recognized that the binding of components with high oxygenophilicity (*e.g.*, hydroxides, oxides and Ru) can facilitate the dissociation of interfacial water and/or adsorption of hydroxyls, thus enhancing the HER/HOR kinetics in alkaline environments.[176,214,215] A recent study showed that the OH groups on the surface of $Ni(OH)_2$ act as mediators, which can attract water molecules to form "metal–OH–H_2O" structures. This dynamic interaction leads to the formation of free O–H bonds in interfacial water, making them more likely to participate in the HER process.[34] These unique perspectives on interfacial water modulation will play a very important role in optimizing further electrocatalytic performance.

6. Conclusion and perspectives

The past decade has witnessed remarkable and continuous advancement in elucidating the behavior and properties of interfacial water in electrocatalysis, fueling growing enthusiasm and establishing this area as a vibrant and rapidly evolving field of research. In this review, a systematic summary of the research progress of interfacial water in electrocatalysis is presented to illustrate the key role of interfacial water in electrocatalytic performance including its unique properties and dynamic behaviors. Simultaneously, advanced characterization techniques and computational methods, such as *in situ* XAS, SERS, SEIRAS and AIMD, are presented, highlighting the significant contributions to the study of interfacial water. More importantly, several effective strategies at the electrolyte and electrocatalyst levels to boost the electrocatalytic performance by interfacial water regulation are highlighted. We hope that this timely and comprehensive overview of interfacial water in electrocatalysis will stimulate further research interest in this area.

While significant advancements have been made in interfacial water-regulated electrocatalysis, several critical challenges remain. In our opinion, future investigations could prioritize the following key directions, as illustrated in Fig. 19.

6.1. Developing more advanced techniques/methods for probing interfacial water

A fundamental understanding of the structure and dynamics of water is key to the study of interfacial water, which requires an accurate analysis of the structure of interfacial water during electrocatalysis, especially for structural differences under different conditions. *In situ* characterization techniques are essential for studying interfacial water behavior but face significant challenges in capturing its dynamic nature and complex interactions during electrocatalysis. However, current methods often lack the temporal resolution to track rapid processes like water adsorption, desorption, and reorganization, or the spatial resolution to map nanoscale heterogeneity. Furthermore, interfacial water behavior is influenced by multiple factors, including electric fields, temperature, reactant concentration and surface properties, making it difficult for single techniques to provide a complete picture.[215] To overcome these challenges, future research should prioritize: (i) developing ultrahigh spatiotemporal resolution techniques (*e.g.*, pump–probe ultrafast lasers and neutron scattering) to capture rapid water dynamics; (ii) designing platforms with multiple physical fields for realistic reaction simulations; (iii) establishing multimodal systems combining complementary techniques (*e.g.*, XAS, SERS, SEIRAS and TEM) for comprehensive analysis of interfacial water.

Theoretical simulations can compensate for the limitations of experimental methods in the study of interfacial water by providing more qualitative and quantitative insights into the structure or properties of interfacial water. AIMD can combine high computational accuracy of quantum chemistry with the advantages of traditional molecular dynamics calculations on time and space scales. Recently, it has attracted increasing attention in exploring the microscopic behavior of complex real systems and revealing their operation mechanisms.[216] Furthermore, as the volume of data generated by *in situ* characterization techniques continues to grow, future research should prioritize the development of efficient quantitative analysis tools to extract valuable physicochemical insights from these large datasets. For instance, machine learning and data mining techniques can be employed to identify patterns in the data, enabling the automated detection and prediction of water molecule behavior and their interactions with catalysts.[217] Additionally, developing integrated platforms capable of handling multidimensional data (*e.g.*, current, potential, temperature and time) and providing intuitive analytical results will

 © 2025 The Author(s). Published by the Royal Society of Chemistry

Open Access Article. Published on 01 2568. Downloaded on 4/1/2569 10:24:58.
This article is licensed under a Creative Commons Attribution-NonCommercial 3.0 Unported Licence.

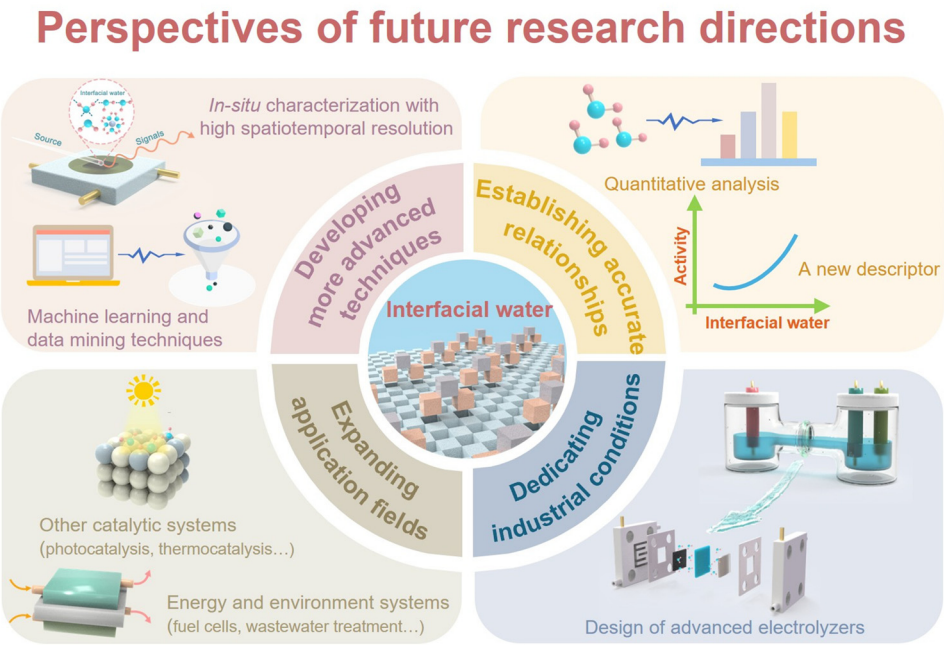

Fig. 19 Perspectives of future research directions on interfacial water for electrocatalysis.

allow researchers to rapidly extract critical information from complex datasets.

6.2. Establishing accurate structure–function–performance relationships for regulating interfacial water

The universalization of the structure–function–performance relationship between interfacial water and electrocatalysis can guide the design of future efficient electrocatalytic systems. Currently, some interfacial water's properties can be regarded as active descriptors for electrocatalytic performance in some cases.[29] For example, it has been shown that under alkaline conditions, the activation energy for water dissociation increases in the order of the interfacial water constructional categories: dangling O–H water < dihedral coordinated water < tetrahedral coordinated water. However, in some reactions involving multiple electrons, like the CO_2RR and NO_3^-RR, such accurate structure–function–performance relationships are not well defined. For example, it is not clear whether a locally ordered or disordered hydrogen bonding environment favors the adaptation of stable transition states and reaction intermediates when reactants are adsorbed onto the electrocatalyst surface. Meanwhile, interfacial water coordinated with these intermediates and interactions with cations increase the difficulty in further understanding the mechanism.[74]

As electrocatalysis deepens into the realm of multi-electron reactions as well as small molecule electrosynthesis, an understanding of "interfacial water effects" is critical. In order to establish an accurate relationship, some methods are recommended as follows: (i) quantitative analysis of interfacial water's functions. By quantifying the functions of interfacial water (*e.g.*, proton transfer, reactant adsorption and hydrogen bonding network dynamics), a quantitative relationship between interfacial water behavior and electrocatalytic performance can be established, thus providing a theoretical basis for the design and optimization of electrocatalytic systems. For example, the rate of proton transfer is quantified by monitoring the pH change of interfacial water in real time through microelectrodes or pH sensors.[218] AIMD simulates the dynamic behavior of interfacial water hydrogen bonding networks, and calculates hydrogen bond lifetimes and recombination rates.[50] (ii) Interfacial water as a new descriptor. With the emerging studies on interfacial water, a new perspective based on interfacial water (besides electrocatalysts) could be provided to describe the electrocatalysis. Correlating functional parameters of interfacial water (*e.g.*, proton transfer rate and reactant adsorption energy) with electrocatalytic performance parameters (*e.g.*, current density and overpotential) allows for a more comprehensive analysis of electrocatalytic performance. This accurate relationship can help to fully understand the electrocatalytic reaction mechanism and design of high-performance electrocatalytic systems. (iii) Rigorous electrochemical testing and accurate performance evaluation are also essential for interfacial water research. In addition to the electrocatalyst, the evaluation of electrocatalytic performance is strongly influenced by external experimental conditions and measurement methods, making it necessary to develop rigorous experimental designs and standardized evaluation protocols with uniform criteria.

6.3. Expanding other application fields for investigating interfacial water

Interfacial water regulation strategies, initially developed for electrocatalysis, also show great potential for cross-disciplinary application in photocatalysis and thermocatalysis, offering opportunities for the catalytic system innovation.[20,219–224]

Open Access Article. Published on 01 2568. Downloaded on 4/1/2569 10:24:58.
This article is licensed under a Creative Commons Attribution-NonCommercial 3.0 Unported Licence.

In photocatalysis, interfacial water not only serves as a solvent or reactant but also modulates charge carrier dynamics by influencing electron–hole transport and reactant adsorption. For instance, water's polarity and solvation effects can alter charge distribution and migration pathways, suggesting that targeted interfacial water regulation could enhance photocatalytic efficiency and stability.[225] Similarly, in thermocatalysis, interfacial water can modify a catalyst's surface properties, including acidity/basicity and intermediate stability, thereby affecting reaction pathways.[226–228] Precise control of water adsorption and desorption behavior may enable the optimization of thermocatalytic activity.

Beyond catalysis, the study of interfacial water has also important application potential in various fields such as energy conversion and environmental remediation. For example, interfacial water modulation can simultaneously enhance the proton conductivity and improve the water management by optimizing the hydration degree of the proton exchange membrane and the water behavior on the electrode surface, thus enhancing the efficiency and stability of fuel cells.[229] In addition, interfacial water plays an important role in environmental remediation, especially in processes such as pollutant degradation and wastewater treatment.[230] Interfacial water has a solvating and activating effect on the catalyst surface, affecting the adsorption and degradation of pollutants. By optimizing the adsorption behavior of water, the stability and reactivity of pollutants on the catalyst surface can be enhanced, thus accelerating the degradation process.

The cross-domain application of interfacial water regulation strategies could facilitate the design of multifunctional catalysts capable of maintaining high performance across electrocatalytic, photocatalytic, and thermocatalytic systems. Such advancements would significantly broaden the application scope of catalytic technologies while optimizing their practical performance.

6.4. Dedicating actual industrial conditions for understanding the "water effect"

Current research on interfacial water's modulation primarily focuses on optimizing the electrocatalytic performance under controlled laboratory conditions, typically involving stability tests of merely several hours at low current densities (*e.g.*, 10 mA cm^{-2}). However, industrial electrolyzer operations demand sustained performance at significantly higher current densities (up to 1000 mA cm^{-2}) over thousands of hours, coupled with exposure to harsh operational environments characterized by strong acid/base corrosion, elevated temperatures and high pressures. These extreme conditions result in the evaporation or decomposition of water molecules, greatly reducing the stability of the electrocatalytic system. Accordingly, water-in-salt systems can largely represent an important segment in the industrialization of electrocatalytic processes and one of the directions for future focused research, due to their advantages of providing ionic conductivity, stabilizing reaction environments, supporting specific reactions and improving reaction efficiencies.[231,232] In addition, there exists an important issue of water management in electrocatalytic units. In large electrocatalytic devices, the uniform distribution of water is a challenge. For instance, in water electrolysis, a dry cathode design is effective in reducing contaminants in hydrogen, but too low a water content can lead to cathode deactivation.[233] Similarly, in CO_2 reduction, which relies on proton exchange membranes, the water-driven effect may lead to cathode deactivation, which in turn leads to a reduction in selectivity.[234] Therefore, the design of advanced flow fields, the development of porous media, the application of efficient water recycling systems, and the development of intelligence and automation in water management have received increasing attention in recent years in water management research.

Although interfacial water modulation strategies have demonstrated remarkable enhancements in electrocatalytic activity and stability under idealized laboratory conditions, their practical applicability in industrial scenarios remains largely unverified. To bridge this gap, future research should prioritize the investigation of interfacial water behavior and its correlation with catalyst structural stability under industrially relevant conditions. This approach will enable the development of robust interfacial water modulation strategies tailored for real-world applications, ultimately facilitating the translation of interfacial water research from laboratory-scale discoveries to industrial-scale implementations.

Conflicts of interest

The authors declare no competing financial interest.

Data availability

No primary research results, software or code has been included and no new data were generated or analysed as part of this review.

Acknowledgements

This work was supported by the Natural Science Foundation for Young Scholars of Jiangsu Province (No. BK20220879), the National Natural Science Foundation of China (No. 22209072 and No. 22479075), the Open Research Fund of Guangdong Advanced Carbon Materials Co., Ltd (No. Kargen-2024B0801), Jiangsu Specially-Appointed Professors and National Natural Science Fund of China for Excellent Young Scientists Fund Program (Overseas).

References

1 N. Vinogradova, T. Pavelsky, J. Farrar, F. Hossain and L. Fu, *Nat. Water*, 2025, **3**, 27–37.
2 J. Qin, W. Duan, S. Zou, Y. Chen, W. Huang and L. Rosa, *Nat. Commun.*, 2024, **15**, 3084.
3 A. Maziotis, R. Garrido, M. Arce and M. Senante, *npj Clean Water*, 2024, **7**, 121.
4 X. Kuang, J. Liu, B. R. Scanlon, J. J. Jiao, S. Jasechko, M. Lancia, B. K. Biskaborn, Y. Wada, H. Li, Z. Zeng,

 © 2025 The Author(s). Published by the Royal Society of Chemistry

Open Access Article. Published on 01 2568. Downloaded on 4/1/2569 10:24:58.
This article is licensed under a Creative Commons Attribution-NonCommercial 3.0 Unported Licence.

Z. Guo, Y. Yao, T. Gleeson, J.-P. Nicot, X. Luo, Y. Zou and C. Zheng, *Science*, 2024, **383**, eadf0630.
5 A. Shih, M. Monteiro, F. Dattila, D. Pavesi, M. Philips, A. Da Silva, R. Vos, K. Ojha, S. Park, O. Heijden, G. Marcandalli, A. Goyal, M. Villalba, X. Chen, G. Gunasooriya, I. McCrum, R. Mom, N. López and M. Koper, *Nat. Rev. Methods Primers*, 2022, **2**, 84.
6 J. Masa, C. Andronescu and W. Schuhmann, *Angew. Chem., Int. Ed.*, 2020, **59**, 15298–15312.
7 C. Liu, F. Chen, B.-H. Zhao, Y. Wu and B. Zhang, *Nat. Rev. Chem.*, 2024, **8**, 277–293.
8 Y. Zhao, J. Xu, K. Huang, W. Ge, Z. Liu, C. Lian, H. Liu, H. Jiang and C. Li, *J. Am. Chem. Soc.*, 2023, **145**, 6516–6525.
9 G. Luderer, S. Madeddu, L. Merfort, F. Ueckerdt, M. Pehl, R. Pietzcker, M. Rottoli, F. Schreyer, N. Bauer, L. Baumstark, C. Bertram, A. Dirnaichner, F. Humpenöder, A. Levesque, A. Popp, R. Rodrigues, J. Strefler and E. Kriegler, *Nat. Energy*, 2021, **7**, 32–42.
10 G. He, J. Lin, F. Sifuentes, X. Liu, N. Abhyankar and A. Phadke, *Nat. Commun.*, 2020, **11**, 2486.
11 Z. Yan, J. Hitt, J. Turner and T. Mallouk, *Proc. Natl. Acad. Sci. U. S. A.*, 2020, **117**, 12558–12563.
12 H. Xia, W. Zhou, X. Qu, W. Wang, X. Wang, R. Qiao, Y. Zhang, X. Wu, C. Yang, B. Ding, L. Hu, Y. Ran, K. Yu, S. Hu, J. Li, H. Cheng, H. Qiu, J. Yin, W. Guo and L. Qiu, *Nat. Nanotechnol.*, 2024, **19**, 1316–1322.
13 C. Chang, Z. Huang and J. Li, *WIREs Comput. Mol. Sci.*, 2016, **6**, 679–693.
14 J. Mellor, *J. Phys. Chem.*, 1903, **7**, 557–567.
15 X. Chen, X. Wang, J. Le, S. Li, X. Wang, Y. Zhang, P. Radjenovic, Y. Zhao, Y. Wang, X. Lin, J. Dong and J. Li, *Nat. Commun.*, 2023, **14**, 5289.
16 K. Sun, X. Wu, Z. Zhuang, L. Liu, J. Fang, L. Zeng, J. Ma, S. Liu, J. Li, R. Dai, X. Tan, K. Yu, D. Liu, W. Cheong, A. Huang, Y. Liu, Y. Pan, H. Xiao and C. Chen, *Nat. Commun.*, 2022, **13**, 6260.
17 Y. Zhu, W. Zhou and Z. Shao, *Small*, 2017, **13**, 1603793.
18 Y. Zhu, Q. Lin, Y. Zhong, H. Tahini, Z. Shao and H. Wang, *Energy Environ. Sci.*, 2020, **13**, 3361–3392.
19 Y. Zhu, H. Tahini, Z. Hu, Z. Chen, W. Zhou, A. Komarek, Q. Lin, H. Lin, C. Chen, Y. Zhong, M. Fernández-Díaz, S. Smith, H. Wang, M. Liu and Z. Shao, *Adv. Mater.*, 2020, **32**, 1905025.
20 J. Shen, A. Aljarb, Y. Cai, X. Liu, J. Min, Y. Wang, Q. Wang, C. Zhang, C. Chen, M. Hakami, J. Fu, H. Zhang, G. Li, X. Wang, Z. Chen, J. Li, X. Dong, K. Shih, K. Huang, V. Tung, G. Shi, I. Pinnau, L. Li and Y. Han, *Nature*, 2025, **13**, 776–782.
21 Y. Wang, Y. Zhu, S. Zhao, S. She, F. Zhang, Y. Chen, T. Williams, T. Gengenbach, L. Zu, H. Mao, W. Zhou, Z. Shao, H. Wang, J. Tang, D. Zhao and C. Selomulya, *Matter*, 2020, **3**, 2124–2137.
22 F. Zhang, Y. Zhu, C. Tang, Y. Chen, B. Qian, Z. Hu, Y. Chang, C. Pao, Q. Lin, S. A. Kazemi, Y. Wang, L. Zhang, X. Zhang and H. Wang, *Adv. Funct. Mater.*, 2022, **32**, 2110224.
23 Z. Liu, Y. Lin, H. Nie, D. Liu, Y. Li, X. Zhao, T. Li, G. Yang, Y. Sun, Y. Zhu, W. Wang, R. Ran, W. Zhou and Z. Shao, *Adv. Funct. Mater.*, 2024, **34**, 2311140.
24 Z. Zhang, T. Wang, Y. Cai, X. Li, J. Ye, Y. Zhou, N. Tian, Z. Zhou and S. Sun, *Nat. Catal.*, 2024, **7**, 807–817.
25 Y. Wang, J. Zhang, J. Zhao, Y. Wei, S. Chen, H. Zhao, Y. Su, S. Ding and C. Xiao, *ACS Catal.*, 2024, **14**, 3457–3465.
26 Z. Tang, C. Li, C. Yan, Q. Zhang, Z. Piao, H. Wang and Y. Zhang, *J. Colloid Interface Sci.*, 2025, **679**, 50–59.
27 Z. Tang, Y. Wang, W. Qian, Z. Piao, H. Wang and Y. Zhang, *J. Colloid Interface Sci.*, 2023, **652**, 1653–1664.
28 S. Zheng, X. Dong, H. Chen, R. Huang, J. Cai and S. Zang, *Angew. Chem., Int. Ed.*, 2025, **64**, e202413033.
29 L. Shen, B. Lu, Y. Li, J. Liu, Z. Huang-fu, H. Peng, J. Ye, X. Qu, J. Zhang, G. Li, W. Cai, Y. Jiang and S. Sun, *Angew. Chem., Int. Ed.*, 2020, **59**, 22397–22402.
30 Y. Chang, L. Kong, D. Xu, X. Lu, S. Wang, Y. Li, J. Bao, Y. Wang and Y. Liu, *Angew. Chem., Int. Ed.*, 2025, **64**, e202414234.
31 L. Wu, W. Huang, D. Li, H. Jia, B. Zhao, J. Zhu, H. Zhou and W. Luo, *Angew. Chem., Int. Ed.*, 2025, **64**, e202413334.
32 S. Li, L. Wu, Q. Liu, M. Zhu, Z. Li, C. Wang, X. Jiang and J. Li, *J. Am. Chem. Soc.*, 2023, **145**, 26711–26719.
33 Y. Hao, L. Wang, H. Huang, H. Zhou, G. Xing, D. Ji, T. Zhang, A. Huang, A. Wang, X. Chen, T. Chen, H. Chen, S. Ramakrishna and S. Peng, *Angew. Chem., Int. Ed.*, 2025, **64**, e202421640.
34 H. Ze, Z. Yang, M. Li, X. Zhang, Y. A, Q. Zheng, Y. Wang, J. Tian, Y. Zhang and J. Li, *J. Am. Chem. Soc.*, 2024, **146**, 12538–12546.
35 I. Yanez, W. Wallace, P. Sebastián-Pascual, V. Climent, J. Feliu and M. Koper, *Nat. Energy*, 2017, **2**, 17031.
36 T. Wang, Y. Zhang, B. Huang, B. Cai, R. Rao, L. Giordano, S. Sun and Y. Horn, *Nat. Catal.*, 2021, **4**, 753–762.
37 Z. Luo, Y. Guo, Y. Qian, L. Zhang, Z. Song, Q. Zhang, C. He and X. Ren, *Adv. Funct. Mater.*, 2024, **34**, 2405881.
38 B. Huang, R. Rao, S. You, K. Myint, Y. Song, Y. Wang, W. Ding, L. Giordano, Y. Zhang, T. Wang, S. Muy, Y. Katayama, J. Grossman, A. Willard, K. Xu, Y. Jiang and Y. Horn, *JACS Au*, 2021, **1**, 1674–1687.
39 C. Schott, P. Schneider, K. Song, H. Yu, R. Götz, F. Haimerl, E. Gubanova, J. Zhou, T. Schmidt, Q. Zhang, V. Alexandrov and A. Bandarenka, *Chem. Rev.*, 2024, **124**, 12391–12462.
40 M. Gebbie, B. Liu, W. Guo, S. Anderson and S. Johnstone, *ACS Catal.*, 2023, **13**, 16222–16239.
41 Y. Wang, S. Zheng, W. Yang, R. Zhou, Q. He, P. Radjenovic, J. Dong, S. Li, J. Zheng, Z. Yang, G. Attard, F. Pan, Z. Tian and J. Li, *Nature*, 2021, **600**, 81–85.
42 G. Shi, T. Lu and L. Zhang, *Nat. Sci. Rev.*, 2024, **11**, nwae241.
43 J. Guo, X. Meng, J. Chen, J. Peng, J. Sheng, X. Li, L. Xu, J. Shi, E. Wang and Y. Jiang, *Nat. Mater.*, 2014, **13**, 184–189.
44 M. Flór, D. Wilkins, M. Puente, D. Laage, G. Cassone, A. Hassanali and S. Roke, *Science*, 2024, **386**, eads4369.
45 C.-Y. Li, J.-B. Le, Y.-H. Wang, S. Chen, Z.-L. Yang, J.-F. Li, J. Cheng and Z.-Q. Tian, *Nat. Mater.*, 2019, **18**, 697–701.

Open Access Article. Published on 01 2568. Downloaded on 4/1/2569 10:24:58.
This article is licensed under a Creative Commons Attribution-NonCommercial 3.0 Unported Licence.

46 X. Chen, X. Li, T. Li, J. Jia, J. Lei, N. Li and H. Luo, *Energy Environ. Sci.*, 2024, **17**, 5091–5101.
47 X. Zheng, B. Zhang, P. Luna, Y. Liang, R. Comin, O. Voznyy, L. Han, F. Arquer, M. Liu, C. Dinh, T. Regier, J. Dynes, S. He, H. L. Xin, H. Peng, D. Prendergast, X. Du and E. Sargent, *Nat. Chem.*, 2018, **10**, 149–154.
48 D. Weinberg, C. Gagliardi, J. Hull, C. Murphy, C. Kent, B. Westlake, A. Paul, D. Ess, D. McCafferty and T. Meyer, *Chem. Rev.*, 2012, **112**, 4016–4093.
49 P. Yang, H. Liu, Q. Jin, Y. Lai, Y. Zeng, C. Zhang, J. Dong, W. Sun, Q. Guo, D. Cao and J. Guo, *J. Am. Chem. Soc.*, 2024, **146**, 210–217.
50 P. Li, Y. Jiang, Y. Hu, Y. Men, Y. Liu, W. Cai and S. Chen, *Nat. Catal.*, 2022, **5**, 900–911.
51 P. Goymer, *Nat. Chem.*, 2012, **4**, 863–864.
52 K. A. Sharp, *Encyclopedia of Life Sciences*, Wiley-VCH, 2001.
53 L. Zheng, M. Chen, Z. Sun, H.-Y. Ko, B. Santra, P. Dhuvad and X. Wu, *J. Chem. Phys.*, 2018, **148**, 164505.
54 L. Novaes, J. Liu, Y. Shen, L. Lu, J. Meinhardt and S. Lin, *Chem. Soc. Rev.*, 2021, **50**, 7941–8002.
55 A. Gomez, W. Thompson and D. Laage, *Nat. Chem.*, 2024, **16**, 1838–1844.
56 G. Zhang, W. Guo, H. Zheng, X. Li, J. Wang and Q. Zhang, *Nat. Commun.*, 2024, **15**, 10845.
57 B. Ye, W. Li, X. Zhang, J. Chen, Y. Gao, D. Wang and H. Pan, *Adv. Mater.*, 2024, **36**, 2402747.
58 R. Butler and A. Coyne, *Chem. Rev.*, 2010, **110**, 6302–6337.
59 J. Davis, B. Rankin, K. Gierszal and D. Amotz, *Nat. Chem.*, 2013, **5**, 796–802.
60 W. Liao, J. Wang, G. Ni, K. Liu, C. Liu, S. Chen, Q. Wang, Y. Chen, T. Luo, X. Wang, Y. Wang, W. Li, T. Chan, C. Ma, H. Li, Y. Liang, W. Liu, J. Fu, B. Xi and M. Liu, *Nat. Commun.*, 2024, **15**, 1264.
61 K. Zhu, J. Ma, L. Chen, F. Wu, X. Xu, M. Xu, W. Ye, Y. Wang, P. Gao and Y. Xiong, *ACS Catal.*, 2022, **12**, 4840–4847.
62 W. Nie, T. Ren, W. Zhao, B. Yao, W. Yuan, X. Liu, Abdullah, J. Zhang, Q. Liu, T. Zhang, S. Tang, C. He, Y. Fang and X. Li, *ACS Appl. Mater. Interfaces*, 2024, **16**, 21828–21837.
63 X. Xu, J. Ma, B. Kui, G. Zhu, G. Jia, F. Wu, P. Gao and W. Ye, *ACS Appl. Nano Mater.*, 2023, **6**, 5357–5364.
64 X. Xu, J. Ma, F. Wu, K. Zhu, H. Zhou, Y. Zhang, X. Li, Y. Zhou, G. Jia, D. Liu, P. Gao and W. Ye, *Inorg. Chem. Front.*, 2022, **9**, 3444–3452.
65 M. Zuhayra, W. Kampen, E. Henze, Z. Soti, L. Zsolnai, G. Huttner and F. Oberdorfer, *J. Am. Chem. Soc.*, 2006, **128**, 424–425.
66 T. Zhang, Q. Ye, Z. Han, Q. Liu, Y. Liu, D. Wu and H. J. Fan, *Nat. Commun.*, 2024, **15**, 6508.
67 Y. Chang, L. Kong, D. Xu, X. Lu, S. Wang, Y. Li, Y. Wang and Y. Liu, *Angew. Chem., Int. Ed.*, 2025, **64**, e202414234.
68 J. Peng, D. Cao, Z. He, J. Guo, P. Hapala, R. Ma, B. Cheng, J. Chen, W. Xie, X. Li, P. Jelínek, L. Xu, Y. Gao, E. Wang and Y. Jiang, *Nature*, 2018, **557**, 701–705.
69 H. Ohtaki and T. Radnai, *Chem. Rev.*, 1993, **93**, 1157–1204.
70 R. Savoj, H. Agnew, R. Zhou and F. Paesani, *J. Phys. Chem. B*, 2024, **128**, 1953–1962.
71 W. Nernst, *Z. Phys. Chem.*, 1888, **2U**, 613–637.
72 B. Hribar, N. Southall, V. Vlachy and K. Dill, *J. Am. Chem. Soc.*, 2002, **124**, 12302–12311.
73 X. Yang, H. Ding, S. Li, S. Zheng, J. Li and F. Pan, *J. Am. Chem. Soc.*, 2024, **146**, 5532–5542.
74 S. Zheng, X. Yang, Z. Shi, H. Ding, F. Pan and J. Li, *J. Am. Chem. Soc.*, 2024, **146**, 26965–26974.
75 M. Toney, J. Howard, J. Richer, G. Borges, J. Gordon, O. Melroy, D. Wiesler, D. Yee and L. Sorensen, *Nature*, 1994, **368**, 444–446.
76 A. Montenegro, C. Dutta, M. Mammetkuliev, H. Shi, B. Hou, D. Bhattacharyya, B. Zhao, S. Cronin and A. Benderskii, *Nature*, 2021, **594**, 62–65.
77 W. Ge, Y. Chen, Y. Fan, Y. Zhu, H. Liu, L. Song, Z. Liu, C. Lian, H. Jiang and C. Li, *J. Am. Chem. Soc.*, 2022, **144**, 6613–6622.
78 X. Li, T. Wang, Y. Cai, Z. Meng, J. Nan, J. Ye, J. Yi, D. Zhan, N. Tian, Z. Zhou and S. Sun, *Angew. Chem., Int. Ed.*, 2023, **62**, e202218669.
79 R. Kronberg and K. Laasonen, *J. Phys. Chem. Lett.*, 2021, **12**, 10128–10134.
80 Y. Wang, H. Yan, H. Cao, J. Chen, H. Yang, J. Zhu and J. Sun, *ACS Catal.*, 2023, **13**, 11080–11090.
81 D. Zhao, F. Liu, X. Duan and D. Sun, *Comput. Mater. Sci.*, 2022, **201**, 110863.
82 S. Shin and A. P. Willard, *J. Chem. Theory Comput.*, 2018, **14**, 461–465.
83 D. Laage, G. Stirnemann, F. Sterpone, R. Rey and J. Hynes, *Annu. Rev. Phys. Chem.*, 2011, **62**, 395–416.
84 Y. Wang, X. Jin, M. Xue, M. Cao, F. Xu, G. Lin, J. Le, W. Yang, Z. Yang, Y. Cao, Y. Zhou, W. Cai, Z. Zhang, J. Cheng, W. Guo and J. Li, *Joule*, 2023, **7**, 1652–1662.
85 A. Shah, Z. Zhang, C. Wan, S. Wang, A. Zhang, L. Wang, A. N. Alexandrova, Y. Huang and X. Duan, *J. Am. Chem. Soc.*, 2024, **146**, 9623–9630.
86 B. Mukherjee, P. K. Maiti, C. Dasgupta and A. K. Sood, *ACS Nano*, 2008, **2**, 1189–1196.
87 K. Jiang, Z. Liu, Z. Wang, F. Xie, X. Yuan and Y. Tan, *Adv. Mater.*, 2025, **37**, 2419644.
88 S. Zhu, R. Yang, H. Li, S. Huang, H. Wang, Y. Liu, H. Li and T. Zhai, *Angew. Chem., Int. Ed.*, 2024, **63**, e202319462.
89 G. Zhang, W. Guo, H. Zheng, X. Li, J. Wang and Q. Zhang, *Nat. Commun.*, 2024, **15**, 10845.
90 T. Shen, L. Spillane, J. Peng, Y. Horn and V. Tileli, *Nat. Catal.*, 2022, **5**, 30–36.
91 M. Konig, J. Vaes, E. Klemm and D. Pant, *iScience*, 2019, **19**, 135–160.
92 S. Wang, E. Zhu, Y. Huang and H. Heinz, *Sci. Adv.*, 2021, **7**, abb1435.
93 S. Cherevko, S. Geiger, O. Kasian, N. Kulyk, J. Grote, A. Savan, B. Shrestha, S. Merzlikin, B. Breitbach, A. Ludwig and K. J. Mayrhofer, *Catal. Today*, 2016, **262**, 170–180.
94 Y. Chen, Z. Tang, Z. Liu, W. Huang, M. Yeh, C. Pao, H. Tao, M. Xu, Z. Dong, L. Yuan, M. Pu, B. Li, G. Yang, Y. Guo, Z. Hu and Y. Zhu, *Adv. Mater.*, 2025, 2504607.

 © 2025 The Author(s). Published by the Royal Society of Chemistry

Open Access Article. Published on 01 2568. Downloaded on 4/1/2569 10:24:58.
This article is licensed under a Creative Commons Attribution-NonCommercial 3.0 Unported Licence.

95 T. Ludwig, J. A. Gauthier, K. S. Brown, S. Ringe, J. K. Nørskov and K. Chan, *J. Phys. Chem. C*, 2019, **123**, 5999–6009.
96 H. Zhang, J. Gao, D. Raciti and A. Hall, *Nat. Catal.*, 2023, **6**, 807–817.
97 A. Wuttig, J. Ryu and Y. Surendranath, *J. Phys. Chem. C*, 2021, **125**, 17042–17050.
98 Y. Wan, M. Pei, Y. Tang, Y. Liu, W. Yan, J. Zhang and R. Lv, *Adv. Mater.*, 2025, **37**, 2417696.
99 X. Liu, J. Meng, J. Zhu, M. Huang, B. Wen, R. Guo and L. Mai, *Adv. Mater.*, 2021, **33**, 2007344.
100 Y. Chen, H. Li, J. Wang, Y. Du, S. Xi, Y. Sun, M. Sherburne, J. Ager III, A. Fisher and Z. Xu, *Nat. Commun.*, 2019, **10**, 572.
101 T. Zheng, C. Shang, Z. He, X. Wang, C. Cao, H. Li, R. Si, B. Pan, S. Zhou and J. Zeng, *Angew. Chem., Int. Ed.*, 2019, **58**, 14764.
102 L. Seitz, C. Dickens, K. Nishio, Y. Hikita, J. Montoya, A. Doyle, C. Kirk, A. Vojvodic, H. Y. Hwang, J. Nørskov and T. Jaramillo, *Science*, 2016, **353**, 1011.
103 W. Du, Y. Shi, W. Zhou, Y. Yu and B. Zhang, *Angew. Chem., Int. Ed.*, 2021, **60**, 7051–7055.
104 H. Xiao, W. GoddardIII, T. Cheng and Y. Y. Liu, *Proc. Natl. Acad. Sci. U. S. A.*, 2017, **114**, E7045.
105 C. Hu, Q. Ma, S. Hung, Z. Chen, D. Ou, B. Ren, H. Chen, G. Fu and N. Zheng, *Chem*, 2017, **3**, 122.
106 L. Näslund, D. Edwards, P. Wernet, U. Bergmann, H. Ogasawara, L. M. Pettersson, S. Myneni and A. Nilsson, *J. Phys. Chem. A*, 2005, **109**, 5995–6002.
107 L. Näslund, J. Lüning, Y. Ufuktepe, H. Ogasawara, P. Wernet, U. Bergmann, L. Pettersson and A. Nilsson, *J. Phys. Chem. B*, 2005, **109**, 13835–13839.
108 E. Hsiao, A. Barnette, L. Bradley and S. Kim, *ACS Appl. Mater. Interfaces*, 2011, **3**, 4236–4241.
109 A. Barnette, D. Asay and S. Kim, *Phys. Chem. Chem. Phys.*, 2008, **10**, 4981.
110 G. Niaura, *Electrochim. Acta*, 2000, **45**, 3507–3519.
111 J. Hower, Y. He and S. Jiang, *J. Chem. Phys.*, 2008, **129**, 215101.
112 J. Zheng, L. Li, H. Tsao, Y. Sheng, S. Chen and S. Jiang, *Biophys. J.*, 2005, **89**, 158–166.
113 Y. He, J. Hower, S. Chen, M. Bernards, Y. Chang and S. Jiang, *Langmuir*, 2008, **24**, 10358–10364.
114 J. Velez, C. Wu, T. Pascal, L. Wan, J. Guo, D. Prendergast and M. Salmeron, *Science*, 2014, **346**, 831–834.
115 L. Jiao, E. Liu, S. Mukerjee and Q. Jia, *ACS Catal.*, 2020, **10**, 11099–11109.
116 H. Zhang, L. Cao, Y. Wang, Z. Gan, F. Sun, M. Xiao, Y. Yang, B. Mei, D. Wu, J. Lu, H. He and Z. Jiang, *ACS Appl. Mater. Interfaces*, 2021, **13**, 47252–47261.
117 M. Cao, K. Liu, Y. Song, C. Ma, Y. Lin, H. Li, K. Chen, J. Fu, H. Li, J. Luo, Y. Zhang, X. Zheng, J. Hu and M. Liu, *J. Energy Chem.*, 2022, **72**, 125–132.
118 Z. Loh, G. Doumy, C. Arnold, L. Kjellsson, S. Southworth, A. Haddad, Y. Kumagai, M. Tu, P. Ho, A. March, R. Schaller, M. Bin, M. Yusof, T. Debnath, M. Simon, R. Welsch, L. Inhester, K. Khalili, K. Nanda, A. Krylov, S. Moeller, G. Coslovich, J. Koralek, M. Minitti, W. Schlotter, J. Rubensson, R. Santra and L. Young, *Science*, 2020, **367**, 179–182.
119 M. Fleischmann, P. J. Hendra and A. J. McQUILLAN, *Chem. Phys. Lett.*, 1974, **26**, 163–166.
120 H. Wang, E. You, R. Panneerselvam, S. Ding and Z. Tian, *Light: Sci. Appl.*, 2021, **10**, 161.
121 D. Jeanmaire and R. Duyne, *J. Electroanal. Chem.*, 1977, **84**, 1–20.
122 L. Palmer, J. Jackson and W. Pierce, *Nature*, 1928, **121**, 501.
123 M. Moskovits, *J. Chem. Phys.*, 1978, **69**, 4159–4161.
124 K. Kneipp, Y. Wang, H. Kneipp, L. Perelman, I. Itzkan, R. Dasari and M. Feld, *Phys. Rev. Lett.*, 1997, **78**, 1667–1670.
125 C. Haynes and R. Duyne, *J. Phys. Chem. B*, 2001, **105**, 5599–5611.
126 J. Li, Y. F. Huang, Y. Ding, Z. L. Yang, S. Li, X. Zhou, F. Fan, W. Zhang, Z. Zhou, D. Wu, B. Ren, Z. Wang and Z. Tian, *Nature*, 2010, **464**, 392–395.
127 Z. Wang, W. Guo, L. Li, B. Luk'yanchuk, A. Khan, Z. Liu, Z. Chen and M. Hong, *Nat. Commun.*, 2011, **2**, 218.
128 M. Kamp, B. Nijs, N. Kongsuwan, M. Saba, R. Chikkaraddy, C. Readman, W. Deacon, J. Griffiths, S. Barrow, O. Ojambati, D. Wright, J. Huang, O. Hess, O. Scherman and J. Baumberg, *Proc. Natl. Acad. Sci. U. S. A.*, 2020, **117**, 14819–14826.
129 M. Osawa and M. Ikeda, *J. Phys. Chem.*, 1991, **95**, 9914–9919.
130 A. Hartstein, J. Kirtley and J. Tsang, *Phys. Rev. Lett.*, 1980, **45**, 201–204.
131 E. Pfitzner, H. Seki, R. Schlesinger, K. Ataka and J. Heberle, *ACS Sens.*, 2018, **3**, 984–991.
132 I. Hill, *Biotechnol. Bioeng.*, 1967, **9**, 1–2.
133 L. Dong, X. Yang, C. Zhang, B. Cerjan, L. Zhou, M. Tseng, Y. Zhang, A. Alabastri, P. Nordlander and N. Halas, *Nano Lett.*, 2017, **17**, 5768–5774.
134 J. Kozuch, K. Ataka and J. Heberle, *Nat. Rev. Methods Primers*, 2023, **3**, 70.
135 Y. Chen and Z. Tian, *Chem. Phys. Lett.*, 1997, **281**, 379–383.
136 K. Ataka, T. Yotsuyanagi and M. Osawa, *J. Phys. Chem.*, 1996, **100**, 10664–10672.
137 Y. Tian, B. Huang, Y. Song, Y. Zhang, D. Guan, J. Hong, D. Cao, E. Wang, L. Xu, Y. Horn and Y. Jiang, *Nat. Commun.*, 2024, **15**, 7834.
138 C. Nyamekye, S. Weibel, J. Bobbitt and E. Smith, *Analyst*, 2018, **143**, 400–408.
139 M. Jin, F. Lu and M. Belkin, *Light: Sci. Appl.*, 2017, **6**, e17096.
140 H. Wang, E. Janzen, L. Wang, J. Edgar and X. Xu, *Nano Lett.*, 2020, **20**, 3986–3991.
141 T. Huhtamäki, X. Tian, J. Korhonen and R. Ras, *Nat. Protoc.*, 2018, **13**, 1521–1538.
142 P. Gao, Y. Ji and G. Hou, *J. Am. Chem. Soc.*, 2025, **147**, 2919–2937.
143 Y. Araki, K. Tsukamoto, R. Takagi, T. Miyashita, N. Oyabu, K. Kobayashi and H. Yamada, *Cryst. Growth Des.*, 2014, **14**, 6254–6260.
144 Á. Cimas, F. Tielens, M. Sulpizi, M. Gaigeot and D. Costa, *J. Phys.: Condens. Matter*, 2014, **26**, 244106.

Open Access Article. Published on 01 2568. Downloaded on 4/1/2569 10:24:58.
This article is licensed under a Creative Commons Attribution-NonCommercial 3.0 Unported Licence.

145 Y. Leng and P. Cummings, *Phys. Rev. Lett.*, 2005, **94**, 026101.
146 T. Pham, D. Lee, E. Schwegler and G. Galli, *J. Am. Chem. Soc.*, 2014, **136**, 17071–17077.
147 M. Tuckerman, K. Laasonen, M. Sprik and M. Parrinello, *J. Chem. Phys.*, 1995, **103**, 150–161.
148 S. Selcuk and A. Selloni, *Nat. Mater.*, 2016, **15**, 1107–1112.
149 R. Réocreux, T. Jiang, M. Iannuzzi, C. Michel and P. Sautet, *ACS Appl. Nano Mater.*, 2018, **1**, 191–199.
150 Y. Wang, S. Li, R. Zhou, S. Zhou, S. Zheng, Y. Zhang, J. Dong, Z. Yang, F. Pan, Z. Tian and J. Li, *Nat. Protoc.*, 2023, **18**, 883–901.
151 H. Khani, A. Santiago and T. He, *Angew. Chem., Int. Ed.*, 2023, **135**, e202306103.
152 S. Hou, L. Xu, X. Ding, R. Kluge, T. Sarpey, R. Haid, B. Garlyyev, S. Mukherjee, J. Warnan, M. Koch, S. Zhang, W. Li, A. Bandarenka and R. Fischer, *Angew. Chem., Int. Ed.*, 2022, **61**, e202201610.
153 M. Waegele, C. Gunathunge, J. Li and X. Li, *J. Chem. Phys.*, 2019, **151**, 160902.
154 R. Rao, B. Huang, Y. Katayama, J. Hwang, T. Kawaguchi, J. R. Lunger, J. Peng, Y. Zhang, A. Morinaga, H. Zhou, H. You and Y. Horn, *J. Phys. Chem. C*, 2021, **125**, 8195–8207.
155 X. Mao, X. Bai, G. Wu, Q. Qin, A. P. O'Mullane, Y. Jiao and A. Du, *J. Am. Chem. Soc.*, 2024, **146**, 18743–18752.
156 P. Xu, R. Wang, H. Zhang, V. Carnevale, E. Borguet and J. Suntivich, *J. Am. Chem. Soc.*, 2024, **146**, 2426–2434.
157 J. Li, X. Li, C. Gunathunge and M. Waegele, *Proc. Natl. Acad. Sci. U. S. A.*, 2019, **116**, 9220–9229.
158 M. Görlin, J. Stenlid, S. Koroidov, H. Wang, M. Börner, M. Shipilin, A. Kalinko, V. Murzin, O. Safonova, M. Nachtegaal, A. Uheida, J. Dutta, M. Bauer, A. Nilsson and O. Morales, *Nat. Commun.*, 2020, **11**, 6181.
159 X. Qin, T. Vegge and H. Hansen, *ACS Catal.*, 2024, **14**, 8168–8175.
160 M. Monteiro, A. Goyal, P. Moerland and M. Koper, *ACS Catal.*, 2021, **11**, 14328–14335.
161 S. Piontek, A. Tuladhar, T. Marshall and E. Borguet, *J. Phys. Chem. C*, 2019, **123**, 18315–18324.
162 X. You, D. Zhang, X. Zhang, X. Li, J. Tian, Y. Wang and J. Li, *Nano-Micro Lett.*, 2024, **16**, 53.
163 M. Monteiro, F. Dattila, N. López and M. Koper, *J. Am. Chem. Soc.*, 2022, **144**, 1589–1602.
164 B. Tang, Y. Fang, S. Zhu, Q. Bai, X. Li, L. Wei, Z. Li and C. Zhu, *Chem. Sci.*, 2024, **15**, 7111–7120.
165 J. Yang, J. Jiao, S. Liu, Y. Yin, Y. Cheng, Y. Wang, M. Zhou, W. Zhao, X. Tong, L. Jing, P. Zhang, X. Sun, Q. Zhu, X. Kang and B. Han, *Angew. Chem., Int. Ed.*, 2024, **63**, e202410145.
166 O. Coskun, Z. Bagbudar, V. Khokhar, S. Dongare, R. Warburton and B. Gurkan, *J. Am. Chem. Soc.*, 2024, **146**, 23775–23785.
167 W. Ni, Y. Guan, H. Chen, Y. Zhang, S. Wang and S. Zhang, *Angew. Chem., Int. Ed.*, 2023, **62**, e202303233.
168 Y. Fan, Y. Chen, W. Ge, L. Dong, Y. Qi, C. Lian, X. Zhou, H. Liu, Z. Liu, H. Jiang and C. Li, *J. Am. Chem. Soc.*, 2024, **146**, 7575–7583.
169 F. Dorchies, A. Serva, D. Crevel, J. Freitas, N. Kostopoulos, M. Robert, O. Sel, M. Salanne and A. Grimaud, *J. Am. Chem. Soc.*, 2022, **144**, 22734–22746.
170 N. Mohandas, T. Narayanan and A. Cuesta, *ACS Catal.*, 2023, **13**, 8384–8393.
171 Q. Sun, N. Oliveira, S. Kwon, S. Tyukhtenko, J. Guo, N. Myrthil, S. Lopez, I. Kendrick, S. Mukerjee, L. Ma, S. Ehrlich, J. Li, W. A. Goddard, Y. Yan and Q. Jia, *Nat. Energy*, 2023, **8**, 859–869.
172 K. Zhao, X. Chang, H. Su, Y. Nie, Q. Lu and B. Xu, *Angew. Chem., Int. Ed.*, 2022, **61**, e202207197.
173 S. Bi, R. Wang, S. Liu, J. Yan, B. Mao, A. Kornyshev and G. Feng, *Nat. Commun.*, 2018, **9**, 5222.
174 J. Snyder, T. Fujita, M. Chen and J. Erlebacher, *Nat. Mater.*, 2010, **9**, 904–907.
175 Y. Li, A. Malkani, R. Gawas, S. Intikhab, B. Xu, M. Tang and J. Snyder, *ACS Catal.*, 2023, **13**, 382–391; R. Gomes, R. Kumar, H. Fejzić, B. Sarkar, I. Roy and C. Amanchukwu, *Nat. Catal.*, 2024, **7**, 689–701.
176 R. Subbaraman, D. Tripkovic, D. Strmcnik, K. Chang, M. Uchimura, A. Paulikas, V. Stamenkovic and N. Markovic, *Science*, 2011, **334**, 1256–1260.
177 A. Goyal and M. Koper, *Angew. Chem., Int. Ed.*, 2021, **60**, 13452–13462.
178 O. Jung, M. Jackson, R. Bisbey, N. Kogan and Y. Surendranath, *Joule*, 2022, **6**, 476–493.
179 P. Li, Y. Jiao, Y. Ruan, H. Fei, Y. Men, C. Guo, Y. Wu and S. Chen, *Nat. Commun.*, 2023, **14**, 6936.
180 S. Zhu, X. Qin, Y. Yao and M. Shao, *J. Am. Chem. Soc.*, 2020, **142**, 8748–8754.
181 A. Buckley, T. Cheng, M. Oh, G. Su, J. Garrison, S. Utan, C. Zhu, F. Toste, W. Goddard and F. Toma, *ACS Catal.*, 2021, **11**, 9034–9042.
182 R. Subbaraman, D. Tripkovic, K. Chang, D. Strmcnik, A. Paulikas, P. Hirunsit, M. Chan, J. Greeley, V. Stamenkovic and N. Markovic, *Nat. Mater.*, 2012, **11**, 550–557.
183 Z. Yang, L. Chen, Y. Yin, C. Wei, Z. Xue and T. Mu, *Energy Environ. Sci.*, 2024, **17**, 8801–8809.
184 W. Zhang, W. Ge, Y. Qi, X. Sheng, H. Jiang and C. Li, *Angew. Chem., Int. Ed.*, 2024, **63**, e202407121.
185 M. Lopez, J. Francisco, M. Costa and J. Anglada, *Nat. Rev. Chem.*, 2020, **4**, 459–475.
186 M. Fang, X. Miao, Z. Huang, M. Wang, X. Feng, Z. Wang, Y. Zhu, L. Dai and L. Jiang, *J. Am. Chem. Soc.*, 2024, **146**, 27060–27069.
187 Y. Zhong, Y. Xu, J. Ma, C. Wang, S. Sheng, C. Cheng, M. Li, L. Han, L. Zhou, Z. Cai, Y. Kuang, Z. Liang and X. Sun, *Angew. Chem., Int. Ed.*, 2020, **59**, 19095–19101.
188 Z. Zhang, S. Banerjee, V. Thoi and A. Hall, *J. Phys. Chem. Lett.*, 2020, **11**, 5457–5463.
189 W. Ge, Y. Zhu, H. Wang, H. Jiang and C. Li, *ACS Catal.*, 2024, **14**, 18156–18166.
190 G. Zhang, M. Munoz and B. J. M. Etzold, *Angew. Chem., Int. Ed.*, 2016, **55**, 2257–2261.
191 R. Jinnouchi and A. B. Anderson, *Phys. Rev. B:Condens. Matter Mater. Phys.*, 2008, **77**, 245417.

 © 2025 The Author(s). Published by the Royal Society of Chemistry

Open Access Article. Published on 01 2568. Downloaded on 4/1/2569 10:24:58.
This article is licensed under a Creative Commons Attribution-NonCommercial 3.0 Unported Licence.

192 Z. Liu, X. Lv, S. Kong, M. Liu, K. Liu, J. Zhang, B. Wu, Q. Zhang, Y. Tang, L. Qian, L. Zhang and G. Zheng, *Angew. Chem., Int. Ed.*, 2023, **62**, e202309319.
193 M. Fan, J. Huang, R. Miao, Y. Mao, P. Ou, F. Li, X. Li, Y. Cao, Z. Zhang, J. Zhang, Y. Yan, A. Ozden, W. Ni, Y. Wang, Y. Zhao, Z. Chen, B. Khatir, C. O'Brien, Y. Xu, Y. C. Xiao, G. Waterhouse, K. Golovin, Z. Wang, E. Sargent and D. Sinton, *Nat. Catal.*, 2023, **6**, 763–772.
194 J. Sun, N. Guo, Z. Shao, K. Huang, Y. Li, F. He and Q. Wang, *Adv. Energy Mater.*, 2018, **8**, 1800980.
195 H. Cai, H. Yang, J. Feng, K. Zhou, C. Liu, Q. Hu and C. He, *Adv. Funct. Mater.*, 2024, **34**, 2404102.
196 H. Huang, L. Xu, S. Zuo, Y. Ren, L. Song, C. Zou, X. Wang, J. Martínez, K. Huang and H. Zhang, *Angew. Chem., Int. Ed.*, 2025, **64**, e202414647.
197 W. Yaseen, M. Xie, B. A. Yusuf, S. Meng, I. Khan, J. Xie and Y. Xu, *Small*, 2024, **20**, 2403971.
198 F. Wei, J. Shen, J. Xie, Z. Luo, L. Shi, T. Isimjan, X. Yang, J. Qiu and B. Wu, *J. Energy Chem.*, 2024, **98**, 472–480.
199 C. Cai, K. Liu, L. Zhang, F. Li, Y. Tan, P. Li, Y. Wang, M. Wang, Z. Feng, D. Meira, W. Qu, A. Stefancu, W. Li, H. Li, J. Fu, H. Wang, D. Zhang, E. Cortés and M. Liu, *Angew. Chem., Int. Ed.*, 2023, **62**, e202300873.
200 L. Zhang, H. Hu, C. Sun, D. Xiao, H. Wang, Y. Xiao, S. Zhao, K. Chen, W. Lin, Y. Shao, X. Wang, C. Pao and L. Han, *Nat. Commun.*, 2024, **15**, 7179.
201 N. Wen, H. Wang, Q. Liu, K. Song, X. Jiao, Y. Xia and D. Chen, *Adv. Sci.*, 2024, **11**, 2403206.
202 N. Gao, D. Han, T. Yang, Q. Meng, X. Wang, C. Liu, J. Ge and W. Xing, *Appl. Catal., B*, 2023, **336**, 122913.
203 S. Zhu, R. Yang, H. J. W. Li, S. Huang, H. Wang, Y. Liu, H. Li and T. Zhai, *Angew. Chem., Int. Ed.*, 2024, **63**, e202319462.
204 J. Yue, Y. Li, C. Yang and W. Luo, *Angew. Chem., Int. Ed.*, 2025, **64**, e202415447.
205 R. Ram, L. Xia, H. Benzidi, A. Guha, V. Golovanova, A. Manjón, D. Rauret, P. Berman, M. Dimitropoulos, B. Mundet, E. Pastor, V. Celorrio, C. Mesa, A. Das, A. Sánchez, S. Giménez, J. Arbiol, N. López and F. Arquer, *Science*, 2024, **384**, 1373–1380.
206 B. Tian, H. Wu, Y. Zhang, C. Chen, K. Abdalla, M. Sendeku, L. Zhou, J. Yu, Y. Wang, Y. Kuang, H. Xu, J. Li and X. Sun, *ACS Catal.*, 2024, **14**, 10904–10912.
207 Z. Wei, J. Ding, Z. Wang, A. Wang, L. Zhang, Y. Liu, Y. Guo, X. Yang, Y. Zhai and B. Liu, *Angew. Chem., Int. Ed.*, 2024, **63**, e202402070.
208 D. Jin, F. Qiao, Y. Zhou, J. Wang, K. Cao, J. Yang, J. Zhao, L. Zhou and H. Li, *Nano Res.*, 2024, **17**, 2546–2554.
209 Q. Guo, Y. Li, Z. Xu and R. Liu, *Adv. Energy Mater.*, 2025, **15**, 2403744.
210 B. You, M. Tang, C. Tsai, F. Abild-Pedersen, X. Zheng and H. Li, *Adv. Mater.*, 2019, **31**, 1807001.
211 Z. Xia and S. Guo, *Chem. Soc. Rev.*, 2019, **48**, 3265–3278.
212 K. Jiang, M. Luo, Z. Liu, M. Peng, D. Chen, Y. Lu, T. Chan, F. de Groot and Y. Tan, *Nat. Commun.*, 2021, **12**, 1687.
213 Y. Yan, J. Lin, K. Huang, X. Zheng, L. Qiao, S. Liu, J. Cao, S. Jun, Y. Yamauchi and J. Qi, *J. Am. Chem. Soc.*, 2023, **145**, 24218–24229.
214 N. Danilovic, R. Subbaraman, D. Strmcnik, K. Chang, A. Paulikas, V. Stamenkovic and N. Markovic, *Angew. Chem., Int. Ed.*, 2012, **124**, 12663–12666.
215 D. Strmcnik, M. Uchimura, C. Wang, R. Subbaraman, N. Danilovic, D. Vliet, A. Paulikas, V. Stamenkovic and N. Markovic, *Nat. Chem.*, 2013, **5**, 300–306.
216 T. Wang, X. He, M. Li, Y. Li, R. Bi, Y. Wang, C. Cheng, X. Shen, J. Meng, H. Zhang, H. Liu, Z. Wang, S. Li, B. Shao and T. Liu, *Nature*, 2024, **635**, 1019–1027.
217 F. Wang and J. Cheng, *Curr. Opin. Electrochem.*, 2025, **49**, 101605.
218 M. Adib, C. Barrett, S. O'Sullivan, A. Flynn, M. McFadden, E. Kennedy and A. O'Riordan, *Biosens. Bioelectron.*, 2025, **275**, 117234.
219 Z. Zhang, Z. Dong, Y. Jiang, Y. Chu and J. Xu, *Chem. Eng. J.*, 2022, **435**, 135014.
220 Z. Dong, Z. Zhang, Y. Jiang, Y. Chu and J. Xu, *Chem. Eng. J.*, 2022, **433**, 133762.
221 K. Mao, Y. Zhang and S. C. Tan, *Nat. Water*, 2025, **3**, 144–156.
222 G. Zhou, H. Xu, H. Song, J. Yi, X. Wang, Z. Chen and X. Zhu, *ACS Catal.*, 2024, **14**, 8694–8719.
223 Z. Dong, B. Li and Y. Zhu, *Energy Fuels*, 2024, **38**, 12387–12408.
224 Z. Dong, B. Li, Y. Zhu and W. Guo, *EES Catal.*, 2024, **2**, 448–474.
225 M. Lu, Y. Du, S. Yan, T. Yu and Z. Zou, *Phys. Rev. Lett.*, 2024, **133**, 258001.
226 X. Zhang, Y. Wan, Y. Wen, Y. Zhu, H. Liu, J. Qiu, Z. Zhu, Z. Sun, X. Gao, S. Bai, Y. Zhang, L. Zhang, X. Yan, J. Zhang, Y. Liu, S. Li and L. Zhao, *Nat. Catal.*, 2025, **8**, 465–475.
227 Y. Hui, L. Wang and F. Xiao, *ACS Nano*, 2025, **19**, 7617–7633.
228 J. Li, L. Ding, Z. Su, K. Li, F. Fang, R. Sun, Y. Qin and K. Chang, *Adv. Mater.*, 2023, **35**, 235535.
229 K. Jiao and X. Li, *Prog. Energy Combust. Sci.*, 2011, **37**, 221–291.
230 X. Liu, Y. Pan, Y. Yao, S. Chen, B. Chen and C. Chu, *Environ. Sci. Technol.*, 2025, **59**, 5406–5414.
231 J. Han, A. Mariani, S. Passerini and A. Varzi, *Energy Environ. Sci.*, 2023, **16**, 1480–1501.
232 J. Yue, J. Zhang, Y. Tong, M. Chen, L. Liu, L. Jiang, T. Lv, Y. Hu, H. Li, X. Huang, L. Gu, G. Feng, K. Xu, L. Suo and L. Chen, *Nat. Chem.*, 2021, **13**, 1061–1069.
233 S. Koch, J. Disch, S. Kilian, Y. Han, L. Metzler, A. Tengattini, L. Helfen, M. Schulz, M. Breitwieser and S. Vierrath, *RSC Adv.*, 2022, **12**, 20778.
234 Q. Bai, L. Xiong, Y. Zhang, M. Ma, Z. Jiao, F. Lyu, Z. Deng and Y. Peng, *EES Catal.*, 2024, **2**, 1228.